Varstrometry for Off-nucleus and Dual Subkiloparsec AGN (VODKA): Methodology and Initial Results with *Gaia* DR2

Hsiang-Chih Hwang[1] , Yue Shen[2,3,4] , Nadia Zakamska[1] , and Xin Liu[2,3]
[1] Department of Physics and Astronomy, Johns Hopkins University, Baltimore, MD 21210, USA
[2] Department of Astronomy, University of Illinois at Urbana-Champaign, Urbana, IL 61801, USA
[3] National Center for Supercomputing Applications, University of Illinois at Urbana-Champaign, Urbana, IL 61801, USA
Received 2019 August 5; revised 2019 November 22; accepted 2019 November 25; published 2020 January 9

Abstract

Gaia's precision astrometry allows systematic identification of optically selected subkiloparsec dual active galactic nuclei (AGNs), off-nucleus AGNs, and small-scale lensed quasars by "varstrometry"—where variability-induced astrometric jitter, i.e., temporal displacements of photocenter in unresolved sources, can be reasonably well detected or constrained. This approach extends systematic searches for small-scale ($\gtrsim$mas) dual and off-nucleus AGNs to the poorly explored regime between $\sim$10 pc and $\sim$1 kpc, with *Gaia*'s full sky coverage and depth to $G \sim 21$. We outline the general principles of this method and calculate the expected astrometric signals from the full time series of photocenter measurements and light curves. We demonstrate the feasibility of varstrometry by using *Gaia* Data Release 2 (DR2) data on a sample of variable pre-main-sequence stars with known close companions. We find that extended host galaxies have a significant impact on the accuracy of astrometric and photometric variability in *Gaia* DR2, a situation to be improved in future *Gaia* releases. Using spectroscopically confirmed Sloan Digital Sky Survey quasars, we present several examples of candidate subkiloparsec off-nucleus or dual AGNs selected from *Gaia* DR2. We discuss the merits and limitations of this method and a follow-up strategy for promising candidates. We highlight *Gaia*'s potential of systematically discovering and characterizing the subkiloparsec off-nucleus and dual AGN population in the entire optical sky.

Unified Astronomy Thesaurus concepts: Quasars (1319); Double quasars (406)

Supporting material: machine-readable tables

1. Introduction

The search for and characterization of the binary supermassive black hole (SMBH) population are important both for understanding galaxy formation and for the prospects of low-frequency gravitational wave detection (e.g., Haehnelt 1994; Jaffe & Backer 2003; Volonteri et al. 2003; Hughes 2009; Centrella et al. 2010; Bogdanović 2015). Following the merger of two galaxies, the two BHs within each of the galaxies may eventually evolve into a bound binary via dynamical friction and interactions with gas and stars (e.g., Begelman et al. 1980; Gould & Rix 2000; Milosavljević & Merritt 2001; Blaes et al. 2002; Yu 2002; Khan et al. 2013; Merritt 2013). Studying SMBH pairs at different evolutionary stages, e.g., from tens of kiloparsec separations at the beginning of the merger to $\lesssim$10 pc scales when the two BHs are gravitationally bound to each other, is important for understanding the impact of galaxy mergers on BH fueling and the dynamical evolution of binary SMBHs (e.g., Colpi & Dotti 2011; Dotti et al. 2012; Volonteri et al. 2016).

Beyond $\sim$kiloparsec scales, pairs of SMBHs within merging galaxies can be systematically identified (Figure 1), if both are accreting as active galactic nuclei (AGNs). One possible observational signature of such pairs is double-lined kinematics of the narrow-line regions surrounding each of the BHs in their galaxy cores. However, in most cases such structure in the narrow emission lines is due to the complex kinematics (e.g., rotation and outflows) of the narrow-line region (e.g., Shen et al. 2011a; Zakamska & Greene 2014; Müller-Sánchez et al. 2016; Yuan et al. 2016). Therefore, the dual AGN nature needs

to be confirmed with spatially resolved imaging and/or spectroscopy (e.g., Liu et al. 2010; Shen et al. 2011a; Fu et al. 2012, 2015a, 2015b; Müller-Sánchez et al. 2016). Another method of identifying kiloparsec-scale dual AGNs is via spatially resolved X-ray observations (e.g., Komossa et al. 2003; Comerford et al. 2015). In addition to dual AGNs, single off-nucleus AGNs, i.e., an inspiraling SMBH pair in which the other member is inactive or obscured (e.g., Barth et al. 2008; Comerford & Greene 2014; Barrows et al. 2017; Tremmel et al. 2018), or spatially offset recoiling SMBHs (i.e., BHs "kicked" from the anisotropic gravitational wave emission following the BH coalescence due to momentum conservation; e.g., Baker et al. 2006; Bogdanović et al. 2007; Civano et al. 2012; Blecha et al. 2016), can also be systematically searched for with these techniques. All these methods are in general sensitive to scales above $\sim$1 kpc, with only one or two serendipitous discoveries of low-redshift dual AGNs at $\sim$500 pc projected separations (e.g., Goulding et al. 2019).

However, it becomes challenging to identify AGN pairs at subkiloparsec scales before the two SMBHs become gravitationally bound owing to the stringent spatial resolution requirement. One spatially resolved method is to search for closely separated flat-spectrum sources with high-resolution Very Long Baseline Interferometry (VLBI) imaging (e.g., Burke-Spolaor 2011), which could be due to compact jets around each of the BHs. There is only one confirmed AGN pair at $\sim$7 pc separation serendipitously discovered with VLBI imaging (Rodriguez et al. 2006), as well as a possible 0.35 pc candidate (Kharb et al. 2017). Candidates of subparsec SMBH binaries can be selected based on the periodicity in the light curves (D'Orazio et al. 2015; Graham et al. 2015a, 2015b;
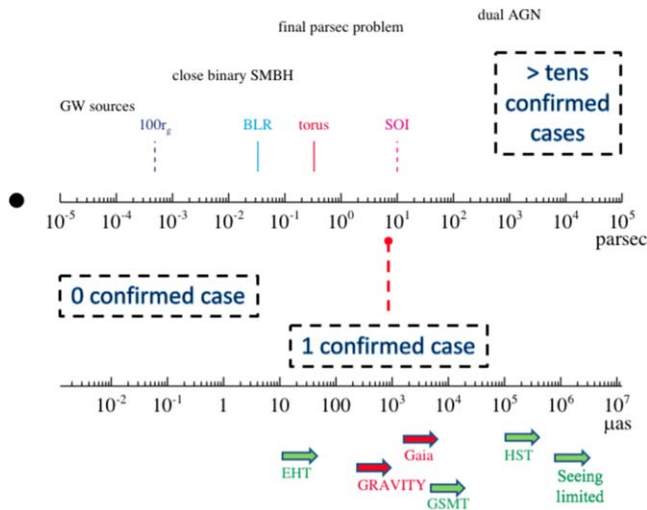
Figure 1. Physical and angular scales around a $10^8 \, M_\odot$ SMBH accreting at a typical Eddington ratio of 0.1 at $z = 1$. The four vertical line segments mark the location of 100 gravitational radii (r_g), the typical distance of the broad-line region (BLR), the typical distance of the dust torus, and the sphere of influence (SOI) of the BH. There are more than a few tens of confirmed dual AGNs with separations greater than ~ 1 kpc. There is only one confirmed $\ll 1$ kpc binary SMBH with a separation of 7 pc (Rodriguez et al. 2006). The minimal spatial scale from different facilities is indicated with the bottom arrows. Direct imaging facilities are indicated in green, and astrometry facilities are indicated in red. Only the Event Horizon Telescope (EHT; Event Horizon Telescope Collaboration et al. 2019) with direct radio interferometry imaging and the GRAVITY instrument on the Very Large Telescope (Gravity Collaboration et al. 2018) with astrometry from IR interferometry can probe smaller scales than *Gaia*. However, neither EHT nor GRAVITY can survey the entire optical sky and probe to the depth of *Gaia*.

Charisi et al. 2016; Zheng et al. 2016; Liu et al. 2019), although such periodic signal can also originate from single BH accretion disks, radio jet precession (Valtonen 2007; Britzen et al. 2018), and/or false positives from stochastic variability (Vaughan et al. 2016; Barth & Stern 2018). Long-term spectroscopic monitoring also helps to reveal the radial velocity variations in subparsec SMBH binaries (e.g., Gaskell 1983; Shen & Loeb 2010; Eracleous et al. 2012; Shen et al. 2013; Liu et al. 2014), and there are some reported candidates (e.g., Li et al. 2016; Guo et al. 2019) for which continued spectroscopic monitoring is required to confirm or rule out the binary hypothesis.

The scales of tens to hundreds of parsecs are of particular interest to binary SMBH evolution. These scales correspond to the late stage of galaxy merger, while the two BHs are on their way to becoming a bound binary. The observed frequency of AGN pairs below kiloparsec scales is essential for testing physical recipes for AGN fueling in galaxy merger simulations and for constraining how fast the BH pair can form a bound BH binary (e.g., Yu et al. 2011; Steinborn et al. 2016; Dosopoulou & Antonini 2017; Kelley et al. 2017; Tremmel et al. 2018). In addition, the subkiloparsec SMBH pair frequency may provide important clues on the physical nature of dark matter particles. For example, in fuzzy dark matter (Hu et al. 2000), a form of dark matter that consists of extremely light scalar particles with masses on the order of $\sim 10^{-22}$ eV, SMBH pairs would never get much closer than $\lesssim 1$ kpc because fuzzy dark matter fluctuations may inhibit the orbital decay and inspiral at kiloparsec scales (Hui et al. 2017).

In this paper, we present a new astrometric technique, motivated by a long history of utilizing astrometry to achieve

super-diffraction-limit applications in astronomy (e.g., Bailey 1998; Shen 2012; Liu 2015, 2016; Stern et al. 2015; Gravity Collaboration et al. 2018). This technique can be used to systematically identify subkiloparsec off-nucleus and dual AGNs and to quantify their frequency using data from the astrometric space telescope, *Gaia* (Gaia Collaboration et al. 2016).

The working principle of this technique is very simple. Consider an unresolved AGN pair (and at least one of them is an unobscured type 1 AGN) at $\lesssim 1$ kpc separations (1 kpc corresponds to $\sim 0''\!.2$ at $z > 0.5$) for which *Gaia* will measure a single-source photocenter.[5] At parsec to subkiloparsec separations, the positions of the two AGNs are essentially fixed given the long ($\gg 100$ yr) dynamical timescale of the pair. Since essentially all AGNs vary stochastically on all timescales with a typical variability amplitude of ~ 0.1–0.2 mag on day to year timescales in the rest-frame UV–optical (e.g., Sesar et al. 2007), the nonsynchronous variation in flux will introduce an astrometric shift in the combined photocenter measured at different observing epochs (Liu 2015, 2016), leading to photocenter variations at the >1 mas level detectable by *Gaia*. This astrometric shift provides a lower limit of the projected physical separation of the AGN pair. However, if the separation is greater than ~ 1–2 kpc ($\sim 0''\!.3$), *Gaia* will likely already resolve the system into two sources given its spatial resolution, scanning direction, and source identification procedure (e.g., Lemon et al. 2017; Ducourant et al. 2018). Therefore, with detected photocenter variations for unresolved sources by *Gaia*, we can identify AGN pairs with projected separations of ~ 5 pc to ~ 1 kpc. Other than direct imaging with VLBI (e.g., Burke-Spolaor 2011), whose feasibility, however, relies on the radio brightness of AGNs and is limited by observing time, the *Gaia* astrometric method represents the only currently viable alternative to constrain the subkiloparsec AGN pair population in a systematic way, and it probes two orders of magnitude smaller angular scales than with *Hubble Space Telescope* (*HST*; see, e.g., Figure 1). The capability of measuring the photocenter to a precision that can be orders of magnitude better than the image resolution underlies this method (e.g., Lindegren 1978).

The validity of this method relies on two factors: an asymmetric intrinsic variability pattern that will cause astrometric jitter in the photocenter of the unresolved source, and sufficient astrometry precision. It is thus distinct from other processes that could also cause photocenter variations not induced by intrinsic variability (such as binary orbital motion, e.g., Bansal et al. 2017, and astrometric microlensing, e.g., Belokurov & Evans 2002). For this reason, here we dub it `varstrometry` (variability+astrometry) for ease of reference and for its general application. A similar idea was applied to unresolved stellar binaries (e.g., Wielen 1996; Makarov & Goldin 2016), which was referred to as the "variability-induced motion" method.

The paper is organized as follows. We first describe the general principles of this astrometric technique and some simulations in Section 2, followed by our initial results on the analysis of data from *Gaia* Data Release 2 (DR2; Gaia Collaboration et al. 2018a) in Sections 3 and 4. We then discuss the implications of our results in Section 5. We summarize our findings and conclude in Section 6. We remind

---

[5] At high redshift, luminous AGNs or quasars often dominate over their host galaxy in the observed-frame optical.

the reader that we are primarily interested in the subkiloparsec regime, where only *Gaia* can provide a systematic search and statistical constraints of such small-scale pairs with its superb astrometric precision, all-sky coverage, and decent optical depth. The smallest pair separation that *Gaia* can potentially recover is ∼5–10 pc. Throughout this paper we adopt a flat ΛCDM cosmology with $\Omega_0 = 0.3$ ($\Omega_\Lambda = 0.7$) and $H_0 = 70$ km s^{-1} Mpc^{-1}.

2. Methods

In this section we present the `varstrometry` technique. Although this technique generally can be applied to any astrometric data, for demonstration purposes we tailor the discussion to *Gaia*, which currently provides the best optical astrometric measurements over the entire sky and to a depth ($G \sim 21$) that is suitable for the systematic searches for dual and offset AGNs.

2.1. The Case of Dual AGNs

In a subkiloparsec pair of SMBHs, if both BHs are actively accreting and appear as unobscured broad-line AGNs, we expect that the photocenter of the unresolved system (two AGNs plus the host galaxy) varies owing to the stochastic variability of both AGNs. If the host galaxy light is negligible, the rms dispersion in the photocenter position, $\sigma_{\rm astro}$, depends on the pair separation D and on the flux contrast between the two AGNs, as well as on their photometric variability amplitude. By Taylor-expanding to the leading order in the fractional flux variation and by assuming statistically independent flux variability from each AGN, we find that we expect

$$\sigma_{\rm astro} \approx \frac{D}{(\bar{f_1} + \bar{f_2})^2}\sqrt{\bar{f_1}^2 \langle \Delta f_2^2 \rangle + \bar{f_2}^2 \langle \Delta f_1^2 \rangle}, \qquad (1)$$

where $\bar{f}$ is the mean flux of the system and Δf is the flux variability. Thus, for an equal-flux pair ($\bar{f_1} = \bar{f_2}$), $\sigma_{\rm astro}$ is linearly proportional to both D and the total rms photometric variability measured from the unresolved system:

$$\sigma_{\rm astro} \approx \frac{D}{2}\frac{\sqrt{\langle \Delta f^2 \rangle}}{\bar{f}}, \qquad (2)$$

in the limit of $\sqrt{\langle \Delta f^2 \rangle} \ll \bar{f}$. Thus, for a 10% rms total flux variability, the astrometric signal is 5% of the pair separation. If we assume the same fractional variability for both AGNs, Equation (2) can be generalized to non-equal-flux pairs:

$$\sigma_{\rm astro} \approx D\sqrt{\frac{2q^2}{(1+q)^2(1+q^2)}}\frac{\sqrt{\langle \Delta f^2 \rangle}}{\bar{f}}, \qquad (3)$$

where $q \equiv \bar{f_2}/\bar{f_1}$. As expected, a larger flux contrast of the two members or lower total photometric variability diminishes the expected astrometric signal. Because of the convolution theorem (e.g., Laury-Micoulaut 1976), these equations remain unchanged when the effect of point-spread function (PSF) is taken into account.

Importantly, the photocenter variations are expected to be bound, aperiodic, and along the direction of the binary, and the largest shifts are expected to be associated with the less frequent, large-amplitude photometric variations. This additional information can be used to confirm the nature of any detected astrometric signals.

To illustrate the relation between the photometric and astrometric variability, we consider the ideal case where the host light is negligible and the unweighted geometric center of the dual AGNs is at the origin. Then, the photocenter of the dual AGN system is the "center of flux." The displacement of photocenter $d_{\rm astro}$ from the origin is determined by the pair separation D and the instantaneous flux contrast $q' \equiv f_2/f_1$:

$$d_{\rm astro} = \frac{D}{2}\frac{q' - 1}{q' + 1}. \qquad (4)$$

Therefore, larger flux changes in one or two of the AGNs induce larger photocenter shifts and dominate the astrometric signals.

Equation (4) also applies to the case (see Section 2.2) where one member of the pair is the host galaxy and the other member is an AGN, regardless of whether or not the host galaxy is extended.

2.2. The Case of Single Off-nucleus AGNs

The varstrometry technique can also be applied to systems where only one member of the SMBH pair is an unobscured AGN, with the other member being obscured or inactive. Such a system appears as an off-nucleus AGN on subkiloparsec scales. An observationally similar but physically different case is that of a recoiling active SMBH after the merger of the two SMBHs. We expect to see photocenter variations in such systems if the host galaxy contributes significant light and if the variability-induced astrometric signal is large enough.

Similar to the dual AGN case, the resulting photocenter variations are linear, bound, and aperiodic. The relation between astrometric rms variability and total photometric rms variability of the unresolved system is (following Equation (1))

$$\sigma_{\rm astro} \approx D\frac{q}{1+q}\frac{\sqrt{\langle \Delta f^2 \rangle}}{\bar{f}}, \qquad (5)$$

where $q = \bar{f_2}/\bar{f_1}$ and $\bar{f_2}$ corresponds to the constant galaxy flux, and $\langle \Delta f^2 \rangle = \langle \Delta f_1^2 \rangle + \langle \Delta f_2^2 \rangle = \langle \Delta f_1^2 \rangle$. In addition, we expect a perfect correlation (in the absence of measurement errors) between the instantaneous photocenter shift and the photometric flux (see Equation (4)), which can be measured with time series of photocenter measurements and photometric light curves. Equation (5) is valid for the case where the host galaxy is extended because host galaxy profiles do not affect the photocenter calculation. Equation (5) remains the same after the convolution with PSF.

It is straightforward to simulate the expected photocenter shifts given the parameters that describe the pair configuration (e.g., projected separation and position angle), flux contrast, variability characteristics, and host contamination. Figure 2 demonstrates the expected astrometric signals for an AGN +galaxy pair. In this mock observation we have used observing parameters that approximately resemble the *Gaia* data, although the exact details are different. A much higher cadence is used to demonstrate the continuous variability in flux and photocenter.

For this simulation, the AGN variability amplitude is typical of the observed values, and the expected photocenter shifts and their strong correlation with the total flux are visually apparent in Figure 2 and detectable with *Gaia*. The resulting photocenter shifts are also consistent with the predictions from
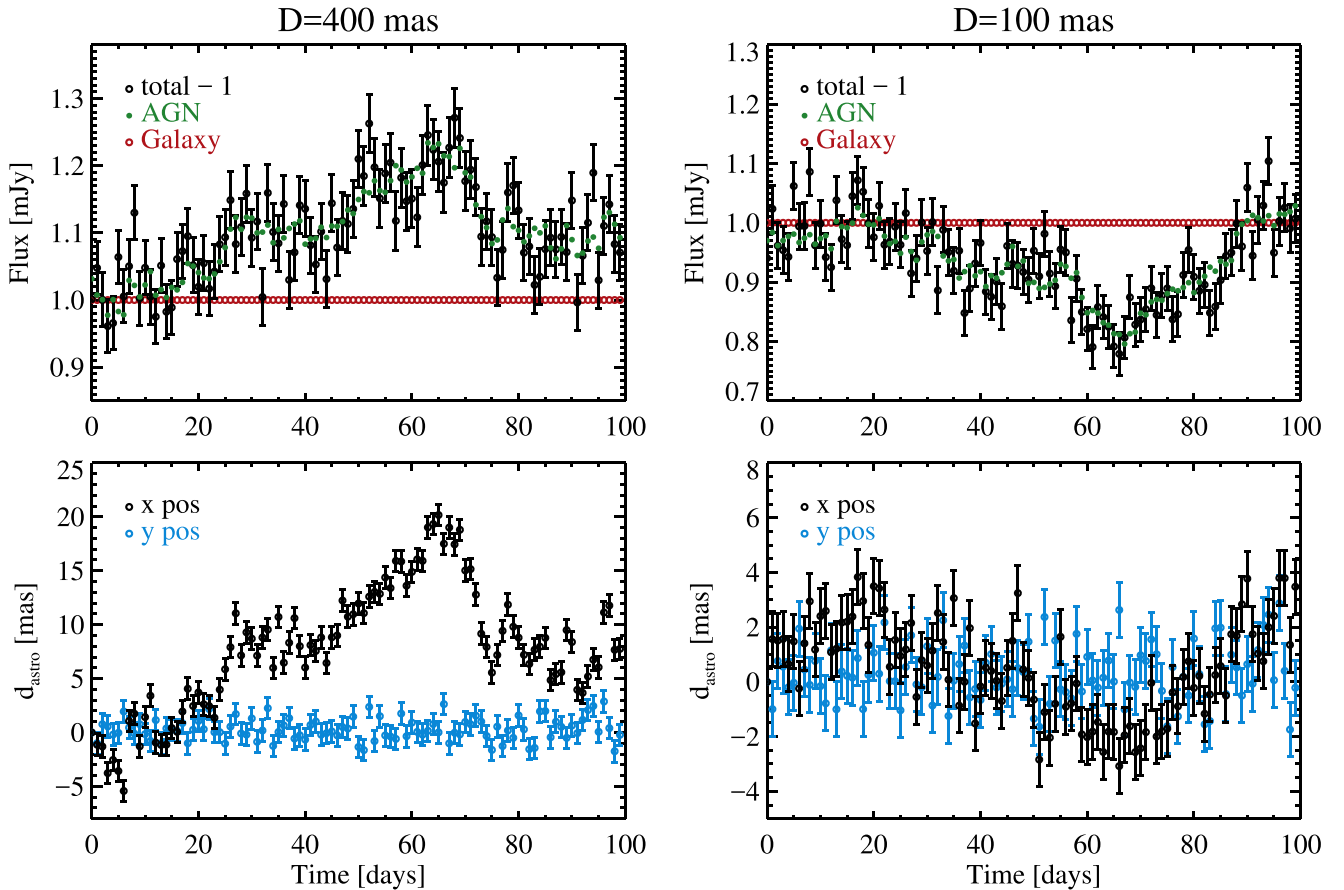
Figure 2. Examples of simulated photocenter and flux variations for an AGN offset from its host galaxy. In this mock observation, we generate light profiles for the AGN assuming a point source and for the galaxy assuming a Sérsic profile (with a Sérsic index $n = 4$ and an effective radius of 10 pixels). The pixel scale of the mock imaging is $0\rlap{.}''1$. We assume a double-Gaussian PSF with the core Gaussian $\sigma = 2$ pixels and the second Gaussian $\sigma = 4$ pixels. The AGN and galaxy pair is along the x-direction with a separation of 4 pixels (400 mas; left panels) and 1 pixel (100 mas; right panels); hence, the system is marginally resolved or unresolved by *Gaia*. The total constant flux from the galaxy is 1 mJy (16.4 AB mag). The AGN light curves are generated using a damped random walk model using typical parameters from MacLeod et al. (2012) and a long-term mean flux of 1 mJy. The flux and photocenter measurements are sampled daily during a 100-day period, with assumed measurement uncertainties of 2% for the total flux and 1 mas for the photocenter positions.

Equation (4). Since the photocenter shift depends linearly on the pair separation, we expect that *Gaia* should be able to detect this astrometric signal even when the pair separation D is several times smaller than that assumed in the simulations. The chance of detecting the photocenter shifts increases when large-amplitude flux variations are captured during the observing period. For example, if the AGN initially has equal flux to the galaxy but during the observing period it varied by a factor of two, then Equation (4) indicates a photocenter shift of $D/6$. Better sampling of the time series of photocenter measurements also helps the correlation analysis with the photometric light curve, even if individual astrometric offsets are marginally detected.

In the case of an offset AGN+galaxy pair, if the constant galaxy flux can be measured through spectral or imaging decomposition, then the observed flux variation and photocenter jitter can be used to derive the projected pair separation D using Equation (4) with linear regression analysis. Figure 3 presents the linear regression between the photocenter measurements and the flux ratios derived for each epoch, for the same examples shown in Figure 2. In these two examples with typical AGN variability, we can reasonably measure the pair separation. Even for cases with smaller pair separation and/or lower variability, the nondetection of astrometric shifts can still be used to place upper limits on the pair separation,

whereas if the AGN varies more than average during the observing period, we can measure smaller pair separations or place tighter upper limits. In a follow-up paper (Shen et al. 2019), we use this method to constrain the population of off-nucleus single AGNs.

3. Application of Varstrometry to *Gaia* DR2

To utilize the full power of the varstrometry technique requires the time series of photocenter measurements and photometric light curves from future releases of *Gaia*. However, even with the cataloged information in *Gaia* DR2, i.e., no time series, we can still use proxies for photometric and astrometric rms variability to test our approach and select initial candidates for follow-up observations. We also examine potential systematics in *Gaia* DR2 that may impact the reliability of varstrometry.

In Section 3.1 we describe the use of *Gaia* DR2 quantities to substitute for the astrometric and photometric rms. In Section 3.2 we investigate the systematics on *Gaia* astrometry and photometry in extended sources. In Section 3.3 we use examples of known binary systems to validate our technique. We defer our analysis on quasars to Section 4. Given *Gaia*'s resolution, scanning strategy, and window sizes in source identification, dual or off-nucleus AGNs on $\gtrsim 0\rlap{.}''3$ (or $\gtrsim 1$ kpc)
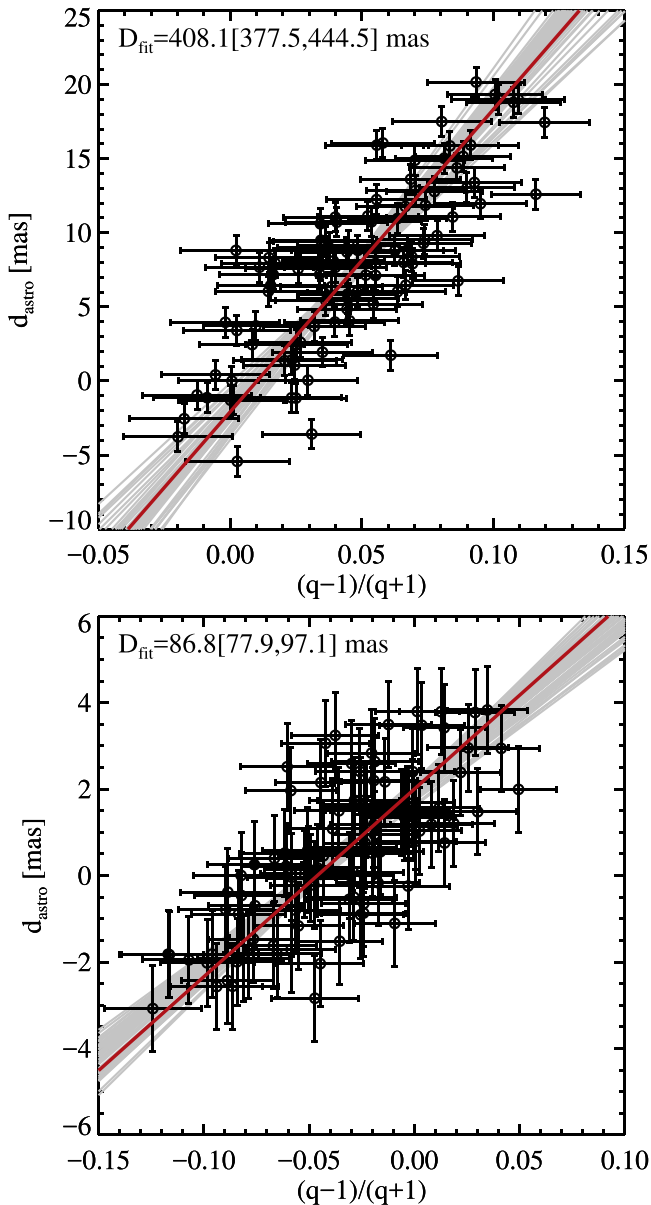
Figure 3. Linear regression between the photocenter shift and the flux ratio measured from each epoch, using the Bayesian regression method in Kelly (2007). The two panels correspond to the two examples shown in Figure 2, with typical AGN variability and pair separations of 400 and 100 mas, respectively. The gray lines are random draws from the posterior distribution of the regression, and the red line indicates the median result. The slope of the regression corresponds to half of the pair separation (see Equation (4)), and the median value and the 16th/84th percentiles of the fitted pair separation are indicated at the top of the panel. For simplicity we did not consider the covariance between the photocenter and flux measurements in the regression fits (i.e., the uncertainties along both axes are treated as independent).

scales are likely resolved into multiple sources in *Gaia*. While not the focus of this paper, we provide a brief discussion on these potential $\gtrsim 1$ kpc off-nucleus or dual AGN systems in Section 4.1.

3.1. Photometric and Astrometric rms Variability in Gaia DR2

Gaia is an optical all-sky survey that is obtaining photometry, positions, parallaxes, and proper motions for stars with magnitudes down to ~21 mag and radial velocities for select bright stars. In *Gaia* DR2 released on 2018 April 25

(Gaia Collaboration et al. 2018a), broad-filter *G*-band magnitudes, blue-band BP magnitudes, red-band RP magnitudes, positions, parallaxes, and proper motions are available for ~1.33 billion objects (five-parameter sources). An additional 0.36 billion objects have available *G*-band magnitudes and positions (two-parameter sources). *Gaia* DR2 is based on data collected between 2014 July 25 and 2016 May 23. In addition to Galactic sources, *Gaia* DR2 contains a large number of extragalactic sources. For example, about half a million *WISE*-selected quasars are cataloged and are used to define the celestial reference frame in *Gaia* (Gaia Collaboration et al. 2018b; Lindegren et al. 2018).

While *Gaia* DR2 has not released the full time series for every source, it does provide an indicator for photometric variability. The photometric errors of the reported mean flux in *Gaia* DR2 are calculated by

$$\text{phot\_g\_mean\_flux\_error} = \sigma_G / \sqrt{\text{phot\_g\_n\_obs}}, \quad (6)$$

where σ_G is the standard deviation of the *G*-band fluxes in the time series. `phot_g_mean_flux_error` and `phot_g_n_obs` are the cataloged *G*-band mean flux error and the number of observations in *G* band, respectively. When a star passes through *Gaia*'s focal plane, there are nine CCDs to measure its photometry in *G* band and the corresponding astrometry, and σ_G is the standard deviation of all CCD-level fluxes in the time series. The photometric precision of individual CCD measurements can be as low as 2 mmag with ~10 mmag systematic uncertainties (Evans et al. 2018). As a result, σ_G contains information about variability on a wide range of timescales, from seconds of *Gaia*'s individual CCD measurements, to hours of the *Gaia* satellite's spinning period, to weeks and years of *Gaia*'s scanning law. For nonvariable sources, σ_G represents the measurement (statistical and systematic) uncertainties in flux; for variable sources, σ_G has contributions from both the intrinsic variability and measurement uncertainties. Indeed, we find that for matched *G* magnitudes, quasars have systematically larger σ_G than stars, due to their intrinsic variability.

Using `phot_g_mean_flux_error` and `phot_g_n_obs`, we compute σ_G and the fractional variability $f_{G,\text{raw}} = \sigma_G / F_G$ for all sources, where F_G is the *G*-band mean flux. To obtain the intrinsic variability estimate, we correct $f_{G,\text{raw}}$ for magnitude-dependent instrumental errors (Evans et al. 2018). The instrumental fractional variability (including statistical errors from photon noise), $f_{G,\text{inst}}$, is computed from the running medians of $f_{G,\text{raw}}$ for a sample of 10 million nearby stars (<500 pc) across all observed *G*-band magnitudes. Using running modes instead of medians gives a difference of only ~10^{-3} in fractional variability, which is not critical for our purposes since the AGN fractional variability is almost always much higher. The intrinsic fractional variability is then computed as $f_G^2 = f_{G,\text{raw}}^2 - f_{G,\text{inst}}^2$. In this definition, f_G^2 may be negative if the source does not have significant variability compared to the running median at its *G*-band magnitude; we set $f_G = 0$ in such cases. For quasars, most of which are fainter than 16 mag, the instrumental correction is from $f_{G,\text{inst}} \sim 0.005$ at $G = 16$ to ~0.08 at $G = 20$. In the following sections, we limit the sample to *G*-band magnitudes brighter than 19.5 mag, where the correction is 6% in fractional variability so we can investigate intrinsic variability at the few percent level. A
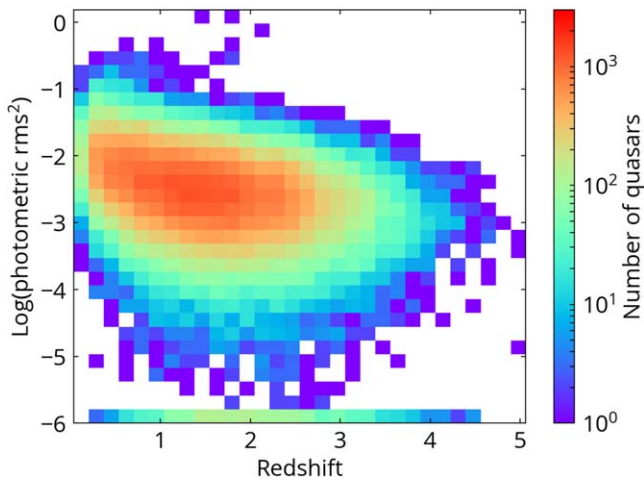
Figure 4. Distribution of SDSS quasars in the fractional photometric rms and redshift plane, color-coded by the number of objects. The photometric rms is estimated using the *Gaia* DR2 flux errors as described in Section 3.1. The trend of decreasing photometric variability with redshift is mainly caused by the $(1 + z)$ time dilation and the general trend that quasars are less variable on shorter (rest-frame) timescales and at higher luminosities (e.g., Vanden Berk et al. 2004; Sesar et al. 2007). This result demonstrates that our proxy for the photometric rms is reasonable.

similar method has been used to obtain variability information from the *Gaia* data set to identify RR Lyrae stars (Belokurov et al. 2017) and eclipsing binaries (Hwang & Zakamska 2019).

Figure 4 displays the fractional photometric rms with redshift for the spectroscopic Sloan Digital Sky Survey (SDSS) quasar sample (see Section 4). The trend of decreasing photometric variability with redshift is mainly caused by the $(1 + z)$ time dilation and the general trend that quasars are less variable on shorter (rest-frame) timescales and at higher luminosities (e.g., Vanden Berk et al. 2004; Sesar et al. 2007). This result demonstrates that our proxy for the photometric rms is reasonable.

The *Gaia* DR2 catalog provides several astrometric quality indicators, including `astrometric_excess_noise` (in units of mas), `astrometric_sigma5d_max` (in mas), `astrometric_chi2_al` (unitless), `astrometric_gof_al` (unitless), `astrometric_excess_noise_sig` (unitless), and the unit weight error introduced in Lindegren et al. (2018). Every indicator has its pros and cons, and we refer the reader to Lindegren et al. (2012, 2018) for more detailed discussion on their properties.

In the following sections, we present the results using `astrometric_excess_noise`. Ideally, if a source is well described by the model (i.e., a single, point-like source in *Gaia* DR2), then the excess noise is 0. Excess noise becomes nonzero when the source has unmodeled astrophysical behaviors (e.g., in binaries) or when the unmodeled instrumental noise is present (Lindegren et al. 2012). Mathematically, `astrometric_excess_noise` is the extra error term added in quadrature to the measurement uncertainty of pixel coordinates in deriving the astrometric solution (Lindegren et al. 2012), and thus it describes the combination of intrinsic astrometric rms and any residual systematic effects. The astrometric jitter induced by `varstrometry`, σ_{astro}, is the intrinsic astrometric rms we want to estimate, and so the `astrometric_excess_noise` quantity provides an upper limit on the intrinsic astrometric rms. Additional benefits of using `astrometric_excess_noise` over other

astrometric quantities include the following: (1) it is in units of mas and has a direct physical interpretation; and (2) it is available regardless of whether the five-parameter astrometric solution is successful or not. Therefore, we use `astrometric_excess_noise` as a proxy (upper limit) for the intrinsic astrometric rms in photocenter. We also test with other astrometric quality indicators, and the main conclusions of this paper remain unchanged.

Faint sources have larger astrometric errors. The standard deviation of along-scan astrometric measurements is >5 mas for sources fainter than 20 mag in G band and is <0.5 mas for G-band magnitudes between 7 and 16.5 mag (Lindegren et al. 2018). We focus on the sample brighter than 19.5 mag in G band, where the standard deviation of along-scan astrometric measurements is <3 mas.

Gaia DR2 has a degree-of-freedom bug when calculating `astrometric_excess_noise` for sources brighter than $G \sim 17$ mag (Lindegren et al. 2018). This bug also propagates to other astrometric quality indicators. Including the effects of the bug, for sources brighter than 13 mag in G band, `astrometric_excess_noise` is underestimated, while for sources with 13–17 mag in G band, `astrometric_excess_noise` is overestimated. This bug is corrected in a magnitude-averaged way in *Gaia* DR2, instead of recomputing the relevant values for every source because the bug was found very late during the data processing of *Gaia* DR2. The majority of our inactive galaxy and quasar samples are fainter than 16 mag, and our results are thus not significantly affected by this detail even if the correction for the bug is not perfect.

3.2. Systematics from Extended Sources

With `varstrometry` we are concerned with distant quasars that are unresolved by *Gaia*. Although unobscured AGNs should present themselves as point sources at *Gaia* resolution, AGNs are hosted by galaxies that are not point sources. Given the scanning law and processing details of *Gaia* astrometry and photometry, extended host galaxies (which are treated as single point sources in *Gaia* DR2) may induce additional systematic uncertainties in the astrometric and photometric measurements.

We use inactive galaxies to investigate how extended host morphology affects the astrometric and photometric rms measurements in *Gaia* DR2. We select star-forming (e.g., emission-line) galaxies from the Portsmouth SDSS DR14 value-added catalog (Thomas et al. 2013). We use emission-line ratios to remove AGNs (Baldwin et al. 1981; Kewley et al. 2001; Kauffmann et al. 2003). After cross-matching with *Gaia* DR2, we end up with a sample of 7692 star-forming galaxies at redshifts <0.6. Inactive galaxies at higher redshifts are too faint for *Gaia*. To quantify the extended structure of the host galaxies, we query the Petrosian half-light radius (R_{50}) in r band from SDSS DR14.

Figure 5 shows the fractional rms photometric variability and `astrometric_excess_noise` from *Gaia* DR2 as a function of R_{50} for the star-forming galaxy sample. Sources with $R_{50} > 1''$ have significantly higher photometric variability and astrometric noise. Specifically, when $R_{50} > 1''$, the measured photometric rms is $\sim 15\%$, even though star-forming galaxies are not expected to vary on the timescales of *Gaia* observations. Therefore, we interpret this photometric rms as the systematic uncertainty for spatially resolved sources. This uncertainty remains roughly constant for R_{50} between $1''$
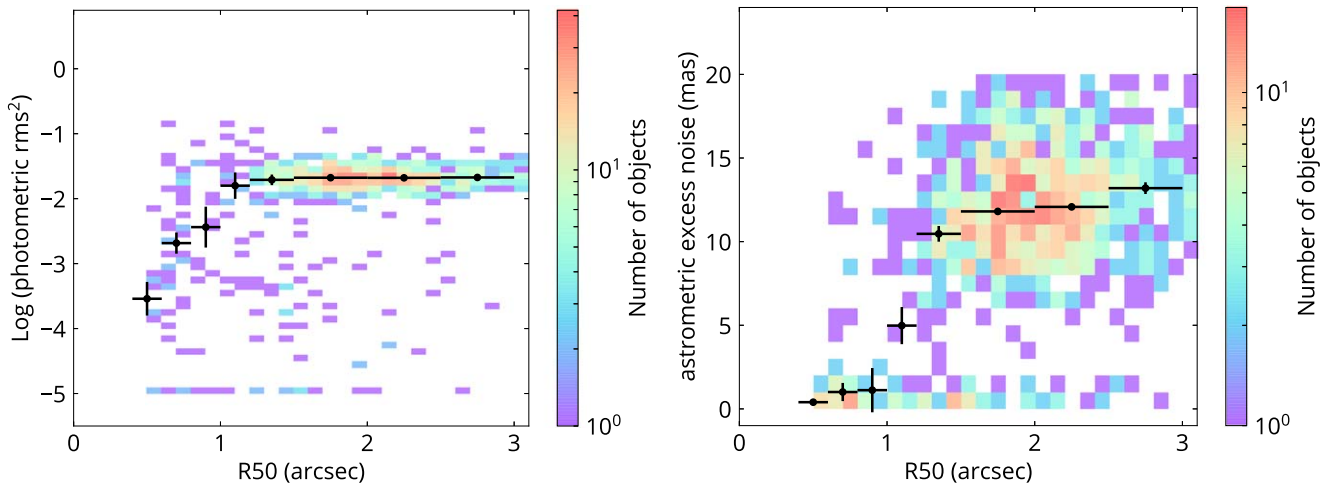
Figure 5. Fractional photometric rms variability (left) and the astrometric excess noise (right) with respect to the Petrosian radius R_{50} in r band for star-forming galaxies. The black markers show the running median in each bin, the x-axis bars indicate the range of the bin, and the y-axis error bars are the standard deviation of mean. In *Gaia* DR2, extended galaxies with $R_{50} > 1''$ have $\sim$10% photometric uncertainty and $\sim$10 mas astrometric excess noise.

and $3''$. The *Gaia*-measured `astrometric_excess_noise` also rises to $\sim$10 mas when $R_{50} > 1''$, which we attribute to the same systematic effect in extended sources.

Nevertheless, these levels of impact on the photometric and astrometric rms estimates are still acceptable, especially for the astrometric rms estimates. For statistical constraints on the off-nucleus and dual AGN population (e.g., Shen et al. 2019), these systematics will not cause significant issues because a $\sim$10 mas systematic uncertainty in the astrometric rms still implies a stringent upper limit of the inferred pair separation. For individual cases, however, we caution that a large astrometric rms signal may be due to extended host morphology.

Figure 5 shows that the impact of host galaxies can be much reduced if we limit the sample to $R_{50} < 1''$. Furthermore, we expect the host-galaxy-induced systematics to be much smaller at high redshift because the host-nucleus flux contrast is much reduced in the observed-frame optical.

3.3. Testing Varstrometry with Galactic Sources

To test the validity of the `varstrometry` technique with *Gaia* DR2, we require known binary (or off-center) systems that are unresolved in *Gaia* (i.e., the spatial offset must be less than $\sim$0$.\!\!''$3), variable in the optical, and with expected astrometric rms greater than the *Gaia* precision of $\sim$1 mas. The preferred test systems would be binary stars, with no complication from extended emission as in galaxies.

There are not many confirmed stellar binary systems that satisfy these requirements simultaneously. The orbital separations of most eclipsing binaries, cataclysmic variables, and triple-star systems are too small. Some spectroscopic binaries might have larger orbits, but they are not necessarily variable. Furthermore, members of the binary need to have comparable fluxes to induce significant astrometric rms. The last requirement rules out most pulsating stars in binary systems because the pulsating member typically dominates the flux.

One suitable test sample for `varstrometry` is pre-main-sequence stars that have close companions because pre-main-sequence stars are known to be variable. We compile such a sample from Ghez et al. (1997) and Nguyen et al. (2012) and references therein, where the close companion is resolved by other facilities (e.g., *HST*) but the system remains unresolved in

Gaia DR2. In some cases, sources remain unresolved in *Gaia* DR2 even if their separations are $>$0$.\!\!''$2. It was pointed out in Arenou et al. (2018) that *Gaia* DR2 has a deficiency in binaries where angular separations are between 0$.\!\!''$12 and 0$.\!\!''$5 (0$.\!\!''$12 is *Gaia*'s theoretical spatial resolution), which may be due to the combination of *Gaia*'s scanning law, limitations of resolving small-separation pairs with high flux contrast, and the quality of astrometric solutions. We then exclude *Gaia*-unresolved systems where the separation is $>$0$.\!\!''$5 because for such wide-separation pairs the light distribution may significantly deviate from the PSF and `varstrometry` may not be the dominant source of astrometric jitter. We further require that `visibility_periods_used` $\geqslant$ 9 so that there are sufficient numbers of *Gaia* observations for astrometric and photometric measurements. This results in 13 systems with companions separated by 0$.\!\!''$03–0$.\!\!''$46. The properties of these 13 systems are listed in Table 1. All of them are in the Taurus–Auriga star-forming region, which is about 140 pc away. Using a nearby sample is important because otherwise it would be difficult to constrain the intrinsic astrometric jitter with noisy measurements of astrophysical proper and parallax motions.

About half (6/13) of the pre-main sequence stars in our sample have intrinsic photometric variability $>$4% in *Gaia* G band. In addition, 9 out of 13 have flux ratios between 0.1 and 10. The ranges of photometric variability and flux ratios make these pre-main-sequence binaries a suitable test sample for `varstrometry`.

Figure 6 shows the comparison between the astrometric rms expected from Equation (3) and the `astrometric_excess_noise` from the *Gaia* DR2 catalog. The uncertainty in the expected rms is computed using the uncertainties of flux ratios and separations from the references listed in Table 1 and assuming that the uncertainty of the fractional photometric rms from *Gaia* is 1%. For cases where the errors of separations and flux ratios are not available, we assume an uncertainty of 5 mas for separations and a 10% relative uncertainty for flux ratios. The flux ratios can change over time, so the flux ratios measured from the literature may be different from those in *Gaia* DR2, but it remains a reasonable first-order estimate. Overall, Figure 6 reveals a reasonably good correlation between the expected and measured intrinsic astrometric jitter
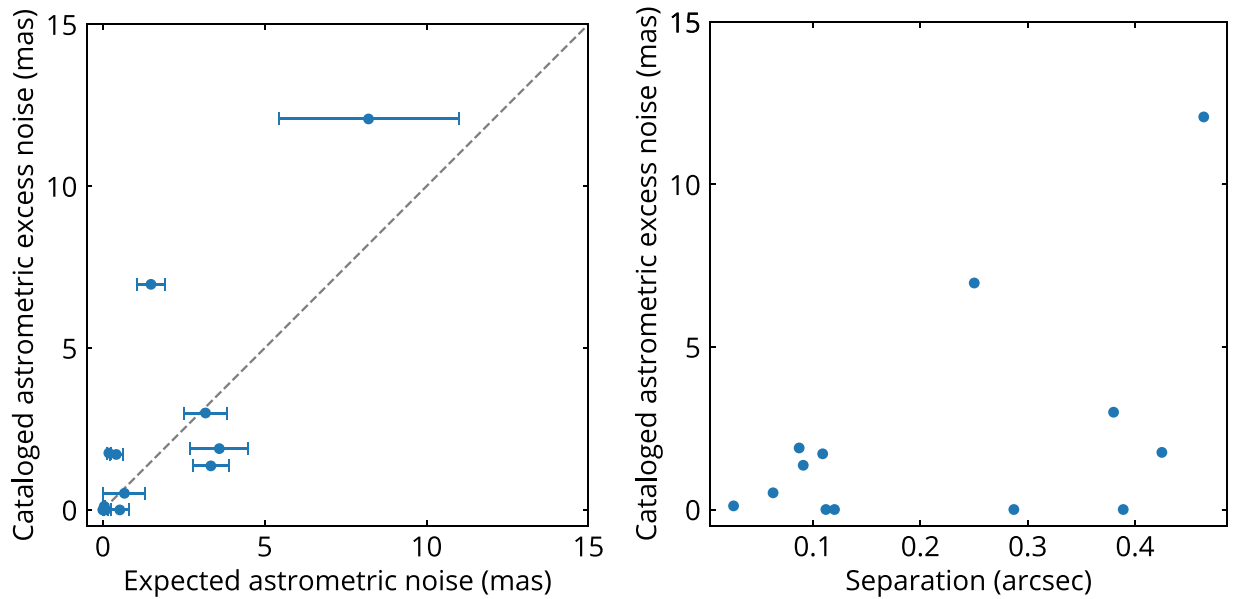
Figure 6. Comparison between the cataloged `astrometric_excess_noise` and the expected astrometric noise from Equation (3) (left panel) and the separation from companions (right panel) for unresolved pre-main-sequence binaries in the Taurus–Auriga star-forming region. The cataloged `astrometric_excess_noise` is broadly consistent with the expected values, while the separation alone only sets the upper limit of the `astrometric_excess_noise` that also depends on variability, in agreement with `varstrometry`.

Table 1
Properties of Pre-main-sequence Stars with Close Companions

Name	AEN[a] (mas)	AENS[b]	Separation (arcsec)	Flux Ratio[c]	$\log(f_G^2)$	Expected AN[d] (mas)	Ref.[e]
DF Tau	1.89	1277.43	0.0871	1.33	−2.14	3.60	4
V773 Tau	0.51	129.46	0.0628	3.5	−2.91	0.67	4
V410 Tau	0.00	0.00	0.2871	265.0	−2.48	0.09	4
GG Tau	6.97	23723.72	0.2502	9.33	−2.72	1.49	4
RX J0430.8+2113	0.00	0.00	0.389	≲0.01	−2.92	0.00	5,6
FF Tau	0.11	4.67	0.026	0.1	−3.77	0.04	3,6
V807 Tau	2.99	2922.86	0.39	0.12	−2.51	3.17	1,6
DI Tau	0.00	0.00	0.12	0.01	−3.55	0.03	2,3,6
RX J0437.2+3108	1.71	1054.44	0.109	0.15	−3.36	0.42	5,6
V827 Tau	1.36	921.19	0.0909	0.31	−1.88	3.34	6
HD286179	0.00	1.09	0.112	0.22	−3.45	0.52	5,6
RX J0452.9+1920	1.76	1785.35	0.425	0.01	−3.01	0.19	5,6
RX J0438.2+2023	12.08	49719.17	0.464	0.87	−2.90	8.21	5,6

Notes.
[a] `astrometric_excess_noise` from *Gaia* DR2.
[b] `astrometric_excess_noise_sig` from *Gaia* DR2.
[c] For sources from Ghez et al. (1997), we adopt the flux ratios in F675W. For other sources, we adopt the flux ratios in *R*-band derived in Nguyen et al. (2012).
[d] Expected astrometric noise computed from Equation (3).
[e] (1) Leinert et al. 1993; (2) Ghez et al. 1993; (3) Simon et al. 1995; (4) Ghez et al. 1997; (5) Kohler & Leinert 1998; (6) Nguyen et al. 2012.

for the pre-main-sequence binary sample, considering the many uncertainties and assumptions in this comparison.

While *Gaia* DR2 provides a dimensionless quantity `astrometric_excess_noise_sig` as an indicator of whether the nonzero astrometric excess noise is significant (Lindegren et al. 2012), we cannot easily convert it to an uncertainty estimate for `astrometric_excess_noise`. For sources where `astrometric_excess_noise` > 1 mas, they all have very high `astrometric_excess_noise_sig`, ranging from ∼900 to ∼50,000, meaning that their astrometric measurements are inconsistent with the single-star model.

We compare `astrometric_excess_noise` and the angular separation of the binaries in the right panel of Figure 6. One may argue that the significant detection of `astrometric_excess_noise` in Figure 6 (left panel) is due to the large companion separation that makes the light profile deviate from a single PSF. However, even for binaries with separations as small as ∼0″.1 *Gaia* detects significant intrinsic astrometric jitter, consistent with the expectation from `varstrometry`.

Even without a good knowledge of the intrinsic flux ratio between the binary components, Figure 6 broadly supports that

we are seeing the intrinsic astrometric jitter caused by `varstrometry` in unresolved binaries. This test also validates the use of Equation (3) to explore `varstrometry` in *Gaia* DR2 even when the full light curve and single-transit astrometric measurements are not available. Furthermore, it demonstrates the more general application of `varstrometry`, e.g., the search for Galactic unresolved variable binary/multiple stars, including pre-main-sequence binaries and triple systems with eclipsing inner binaries.

3.4. Testing Varstrometry with Extragalactic Sources

We now examine the few confirmed dual or off-nucleus AGN systems reported in the literature with *Gaia* data. The pair separations in these systems satisfy the requirements for `varstrometry` with *Gaia* DR2.

CXOC J100043.1+020637 (also known as CID-42) is a double-nucleus AGN, and one of the nuclei is an unobscured type 1 AGN (Civano et al. 2010), so there is expected optical variability. The separation of the two nuclei is $\sim 0\rlap{.}''4$ (~ 2.5 kpc). *Gaia* DR2 does not resolve the system into two objects, and the single *Gaia* source does have high `astrometric_excess_noise` of 13 mas. It has a fractional photometric variability of $f_G = 20\%$. Adopting a host-to-AGN flux ratio of $q = 2/3$ from Civano et al. (2010), we estimate an expected astrometric rms of ~ 32 mas using Equation (5), which is larger than the reported `astrometric_excess_noise`. However, given the low redshift of CID-42, the *Gaia* photometric rms may be overestimated owing to the extended host. Indeed, the light curves from the Dark Energy Survey Y3 data (Diehl et al. 2016) covering roughly the same period as *Gaia* DR2 indicate an intrinsic photometric rms of only $\sim 8\%$ in *g* and *i* bands (Y. Chen, private communication), which would result in an expected astrometric rms of ~ 13 mas, almost in perfect agreement with *Gaia* `astrometric_excess_noise`. Of course, we are unable to rule out that the *Gaia* DR2 astrometric rms measurement is also affected by the extended host galaxy because of its low redshift of $z = 0.359$.

The radio galaxy 0402+379 has a 7 pc AGN binary reported in Rodriguez et al. (2006), but its host galaxy is too extended and smooth in optical, and therefore it is not considered as a point-like source cataloged in *Gaia* DR2.

SDSS J092455.24+051052.0 is a dual AGN with a projected angular separation of $0\rlap{.}''4$ (Liu et al. 2018). While it does have high astrometric excess noise of 15 mas, it may be due to its extended host galaxy because its redshift is only $z = 0.1495$ and it is a type 2 AGN where strong photometric variability is not expected.

4. Varstrometry of Quasars in *Gaia* DR2

We now proceed to investigate the photometric and astrometric rms properties of quasars using *Gaia* DR2. We emphasize that in this initial study we will not be able to confirm any subkiloparsec dual/off-nucleus AGNs or small-scale lenses. Instead, we mainly use this exercise to understand potential systematics and to formulate our follow-up strategy for potential candidates (Section 5.2).

Our main quasar sample includes $\sim 500,000$ spectroscopically confirmed quasars from the SDSS DR7 quasar catalog (Shen et al. 2011b) and the SDSS DR14 quasar catalog (Pâris et al. 2018). In Section 4.4, we also consider a photometric quasar sample selected using data from the *WISE* (Wright et al. 2010)

survey and presented in Secrest et al. (2015), to increase the overlap with the *Gaia* sky coverage.

4.1. Quasars with Multiple Gaia Source Detections

We cross-match the SDSS quasars with *Gaia* DR2 with a matching radius of $3''$, resulting in $\sim 350,000$ quasars with *Gaia* matches out of the $\sim 500,000$ parent quasars. The remaining SDSS quasars are too faint for *Gaia* DR2's detection limit (~ 21 mag in *G* band). During the cross-match, we keep all *Gaia* sources within $3''$ (i.e., there could be multiple *Gaia* sources within $3''$) because *Gaia* may resolve dual/off-nucleus AGNs and lensed quasars separated by $\gtrsim 0\rlap{.}''2$.

We first investigate the multiple-quasar systems where each member is spectroscopically confirmed as a quasar in SDSS. There are 16 such systems in total: 11 of them are lensed/dual quasar candidates where the redshifts of the members are very close ($\Delta z < 0.1$); three have members at different redshifts that are projected quasar pairs; one system contains two quasars, SDSS J123401.31+063214.9 and SDSS J123401.24+063212.1, with nearly identical redshifts but different colors. The last system, SDSS J114653.06+164425.3, turns out to be an SDSS imaging processing problem, and it is in fact a single quasar. In these cases, quasars may have *Gaia* cross-matches of the other member, so we manually identify the correct *Gaia* matches for individual members.

Next, we investigate single SDSS quasars with multiple matches in the *Gaia* database. Out of the $\sim 350,000$ quasars with at least one *Gaia* match within $3''$, one quasar has four matched *Gaia* sources, five have three *Gaia* sources, and 1600 have two *Gaia* sources within $3''$. In these multiply matched cases, the closest match is usually the correct match to the quasar, while others are close companions. The one having four *Gaia* sources is a well-known quadruply imaged, lensed quasar PG 1115+080 (SDSS J111816.94+074558.2) at $z = 1.73$ (e.g., Weymann et al. 1980; Young et al. 1981; Kristian et al. 1993). Out of the five sources having three *Gaia* matches, four have resolved members with significantly different optical colors in Pan-STARRS (Chambers et al. 2016) images, while the last one (SDSS J141546.24+112943.4) is a known quadruply lensed quasar (Magain et al. 1988).

For the 1600 sources having two *Gaia* matched sources, they can be either dual AGNs or off-nucleus AGNs on $\gtrsim 1$ kpc scales, gravitational lensed quasars, projected quasar pairs, or quasars close in projection to foreground stars. Figure 7 shows the distributions of the *Gaia* matched sources for these 1600 quasars in the proper motion, photometric variability, and color space, color-coded by the distance from the SDSS position. In *Gaia* DR2, BP and RP bands are measured from the sum of fluxes within a 3.5×2.1 arcsec^2 window (no deblending treatment), so the BP − RP color in Figure 7 represents the average color within such a window around the source. On average, *Gaia* sources with larger matched separations have higher proper motions, tend to be less variable, and have redder colors. Therefore, we conclude that most of these large-separation sources are Milky Way stars. Nevertheless, there are many sources that are consistent with AGNs in terms of photometric variability, proper motion, and color. These are promising dual AGN candidates on $\gtrsim 1$ kpc scales already resolved by *Gaia* DR2.

Figure 8 presents a 3.7 kpc dual AGN candidate SDSS J000710.01+005329.0 at $z = 0.32$ that has two *Gaia* source detections separated by $0\rlap{.}''79$. The *i*-band image (left panel)
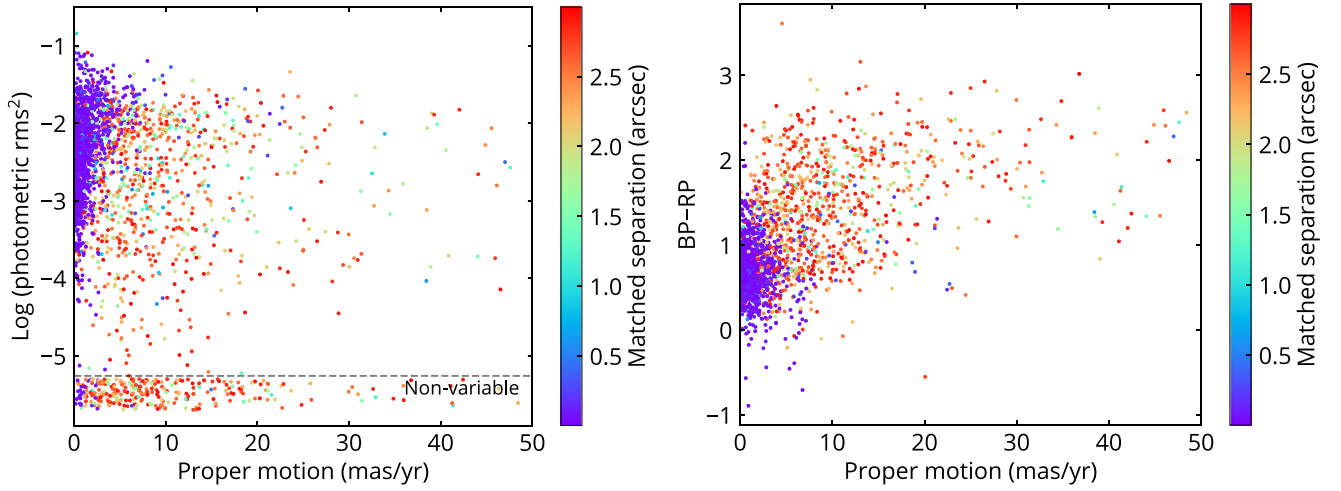
Figure 7. Left: fractional photometric variability vs. total proper motion for SDSS quasars that have two *Gaia* matches within 3″. For sources where the photometric rms is below the instrumental level, we place them below the dashed line with some small random vertical offsets. *Gaia* matches with separations <0.″3 have small proper motions and significant variability, while sources with larger matched separations have higher proper motions, tend to be less variable, and have redder colors, suggesting that these larger-separation matches are likely to be foreground stars. Nevertheless, there are many systems where the multiple *Gaia* matches within 3″ are consistent with AGNs in terms of photometric variability, proper motion, and color. These are promising dual AGN candidates on ≳1 kpc scales that are already resolved by *Gaia*.
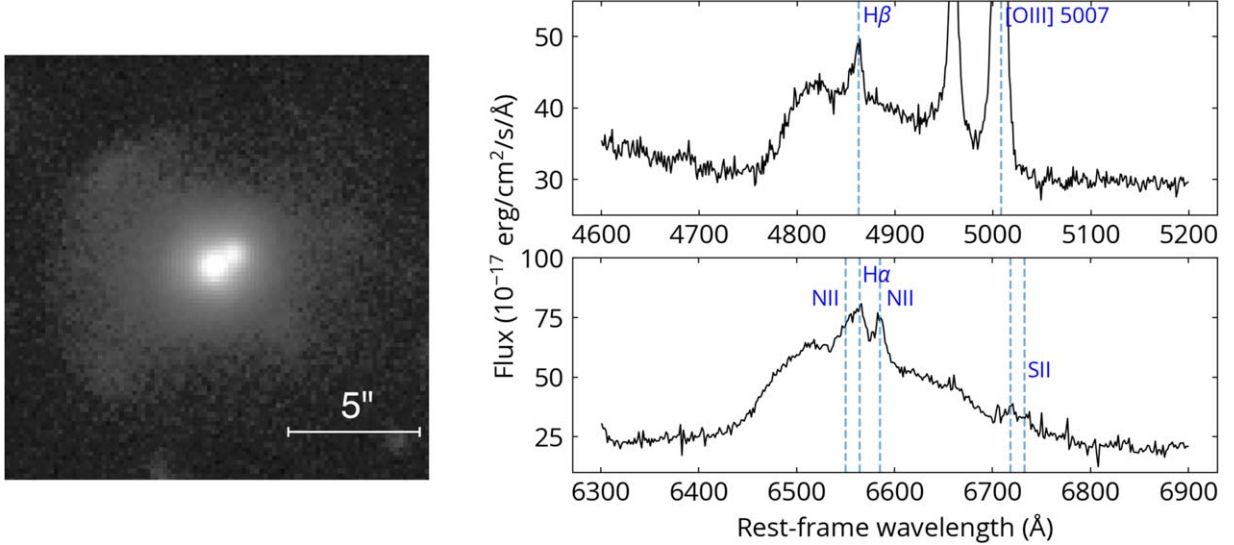

Figure 8. HSC *i*-band image (left panel; north/east is up/left) and SDSS spectrum (right panel) of SDSS J000710.01+005329.0, a quasar at $z = 0.32$. *Gaia* DR2 detects two sources separated by 0.″79 in the source, coincident with the two cores visible in the HSC image. There is also a faint extended shell-like structure indicative of an evolved merger. Its SDSS spectrum shows disk-emitter-like features in the broad Balmer lines. This is likely a dual AGN with a projected separation of 3.7 kpc.

from the Hyper Supreme-Cam (HSC) Survey DR2 (Aihara et al. 2019) clearly shows two resolved cores and a more extended faint structure indicative of an evolved merger. Its SDSS spectrum (right panel) shows disk-emitter-like features in the broad Balmer lines (Eracleous & Halpern 1994; Strateva et al. 2003). The northwest *Gaia* source has `astrometric_excess_noise` = 0 and a fractional photometric variability of $\log(f_G^2) = -2.8$, and the southeast one has `astrometric_excess_noise` = 0.77 mas and a fractional photometric variability of $\log(f_G^2) = -1.6$. Because the source is resolved by *Gaia*, varstrometry should not lead to astrometric rms, consistent with the <1 mas astrometric excess noise for these two *Gaia* sources. The northwest *Gaia* source only has a two-parameter astrometric solution (i.e., R.A. and decl.), while the southeast one has a five-parameter

solution with proper motions and parallax consistent with zero. This example demonstrates that it is desirable to further investigate quasars that have multiple *Gaia* detections since they may be promising dual AGN candidates resolved by *Gaia*. The spatial resolution requirement to resolve these systems is well within the reach of ground-based adaptive optics or *HST* imaging, as well as radio interferometry.

4.2. Quasars with Significant Gaia Parallax or Proper Motion

We now investigate quasars with significant parallaxes and proper-motion detections in *Gaia* DR2. Ideally, quasars should have zero parallaxes and zero proper motions. Quasars with significant parallaxes and proper motions may inform us of sample contamination and systematics, or can be due to

interesting physical causes, such as `varstrometry`. We keep in mind that `astrometric_excess_noise` is a more generally applicable indicator of astrometric rms than parallax/ proper motion, as it is available even for sources with two-parameter astrometric solution only (i.e., no available parallax or proper-motion measurements). However, under certain circumstances, the intrinsic astrometric rms may be mistakenly reported as a valid astrometric solution for parallax and proper-motion measurements, with negligible reported `astrometric_excess_noise` from *Gaia* DR2. The purpose of this subsection is to examine cases where *Gaia* reports significant parallaxes and proper-motion detections for quasars, regardless of their `astrometric_excess_noise` values.

We select quasars that have positive parallaxes by (1) `parallax_over_error > 5`, i.e., parallax inconsistent with zero at 5σ; and (2) the *Gaia*-SDSS separation $<1''$ to reduce contamination from foreground stars (see Figure 7). For each quasar, we consider all *Gaia* matches satisfying the above criteria to include potential dual AGNs resolved by *Gaia*. This results in 25 SDSS objects, where 15 have single *Gaia* matches and 10 have two *Gaia* matches within $1''$. To determine the physical nature of these sources, we investigate their SDSS spectra and their optical colors in SDSS and Pan-STARRS 1.

For sources with single *Gaia* matches, we classify them into three categories: (1) genuine quasars where broad emission lines are identifiable in SDSS spectra; (2) sources with nearly featureless continuum in SDSS spectra; and (3) magnetized white dwarfs where the line splitting from the Zeeman effect is identifiable. Category 2 can either be weak-line quasars or DC (no absorption lines) white dwarfs (Collinge et al. 2005).

Out of the 15 SDSS objects with significant nonzero parallaxes and single *Gaia* matches, 9 are in category 1, 4 are in category 2, and 2 are in category 3. We compute the significance of their proper motions and find that sources in categories 2 and 3 have nonzero proper motions at $\gtrsim 20\sigma$, while sources in category 1 have significance less than 10σ (only one is above 5σ). By using their parallaxes to compute the *G*-band absolute magnitudes, we find that sources in categories 2 and 3 are consistent with the location of white dwarfs in the color–absolute magnitude diagram, while sources in category 1 are mostly scattered between the white dwarf track and the main sequence of stars. Therefore, we conclude that sources in categories 2 and 3 are mostly (if not all) white dwarfs misclassified as quasars in the SDSS quasar catalog and category 1 is a clean quasar sample.

For the 10 SDSS objects that have two close *Gaia* matches within $1''$, only one of the two *Gaia* matches has a significant nonzero parallax. We investigate their proper motions and optical colors. We find that five *Gaia* sources with nonzero parallaxes have nonzero proper motions at $>10\sigma$ and red optical colors of BP – RP >0.9 whenever applicable. Furthermore, the SDSS spectra of two of these systems show identifiable M-dwarf spectral features (SDSS J092853.51 +570735.3 and SDSS J014349.15+002128.3). We conclude that these five quasars are in close projection to foreground stars. The other five *Gaia* matches to SDSS quasars with nonzero parallaxes have bluer optical colors of BP − RP < 0.8 (similar to *Gaia* matches with zero parallaxes) and less significant proper motions ($<10\sigma$). They may be multiply lensed quasars, although we cannot rule out the possibility that they are blue foreground stars.

We conclude with a sample of 14 genuine quasars that have nonzero parallaxes, where nine have single *Gaia* matches and five have two *Gaia* matches within $1''$. Their redshifts range from 0.44 to 3.5. For the nine quasars with single *Gaia* matches within $1''$ the astrometric solution is not affected by crowding. Out of these nine quasars, six have `visibility_periods_used` $\geqslant 9$, so they should have sufficient numbers of observations to derive reliable parallaxes. Three out of nine have `astrometric_excess_noise > 1 mas`, suggesting that these sources may have unusual behaviors in their astrometric measurements. These nine quasars are good candidates for `varstrometry`-selected subkiloparsec dual/ off-nucleus AGNs.

We also investigate quasars that have nonzero proper motions. We select candidates with (1) total proper motion 5σ inconsistent with 0 and (2) *Gaia*-SDSS cross-match separation $<1''$. The selection results in 51 SDSS quasars. This sample contains 11 systems that have nonzero parallaxes, which we have discussed above, but none of them are considered as genuine quasars by our previous classification. Excluding these 11 nonzero parallax systems, we end up with 40 SDSS quasars that have nonzero proper motions, with 19 of them having a single *Gaia* source and 21 having two *Gaia* sources within $1''$.

For quasars that have nonzero proper motions, we check their SDSS spectra, and for those having multiple *Gaia* detections, we check whether the detected sources have similar colors in order to classify them as either foreground stars or lensing candidates. Out of the 19 sources with single *Gaia* source detection, the SDSS spectra show that 8 are genuine quasars, 7 have prominent stellar features (F, G, K, M stars) with some trace of AGN features indicating star+quasar superposition, 1 has peculiar spectral features that might be a carbon star (SDSS J093306.61+500544.4), and 3 are featureless.

For the 21 quasars with nonzero proper motions and two matched *Gaia* sources, the SDSS spectra of 10 objects have prominent stellar spectral features and therefore are super-positions with foreground stars. For the remaining 11 quasars, all of them have AGN-dominant spectral features with little trace of foreground stars. Some of them are known lensing systems, for example, SDSS J091127.61+055054.1 (RX J0911.4+0551).

We compile tables, Pan-STARRS $g+z$ optical images, and SDSS spectra for genuine quasars that have significant nonzero parallaxes or proper motions in the Appendix. We exclude white dwarfs misclassified as quasars and quasar–star superpositions.

It is unclear why some genuine quasars and lensing systems have nonzero parallaxes and/or proper motions. `Varstrometry` could be one physical cause, i.e., the astrometric rms is mistaken as a valid astrometric solution. Alternatively, the "detected" parallaxes and/or proper motions are due to systematics, such as extended hosts. Nevertheless, quasars with significant parallaxes and proper motions are rare, only $\sim 0.01\%$ of the entire sample; thus, we must be careful with the possibility that these nonzero parallaxes and proper motions are simply statistical outliers. To confirm the nature of these systems, we need independent follow-up observations that can potentially resolve their small-scale structure, or we must wait for future *Gaia* releases to provide more information and reduced systematics.
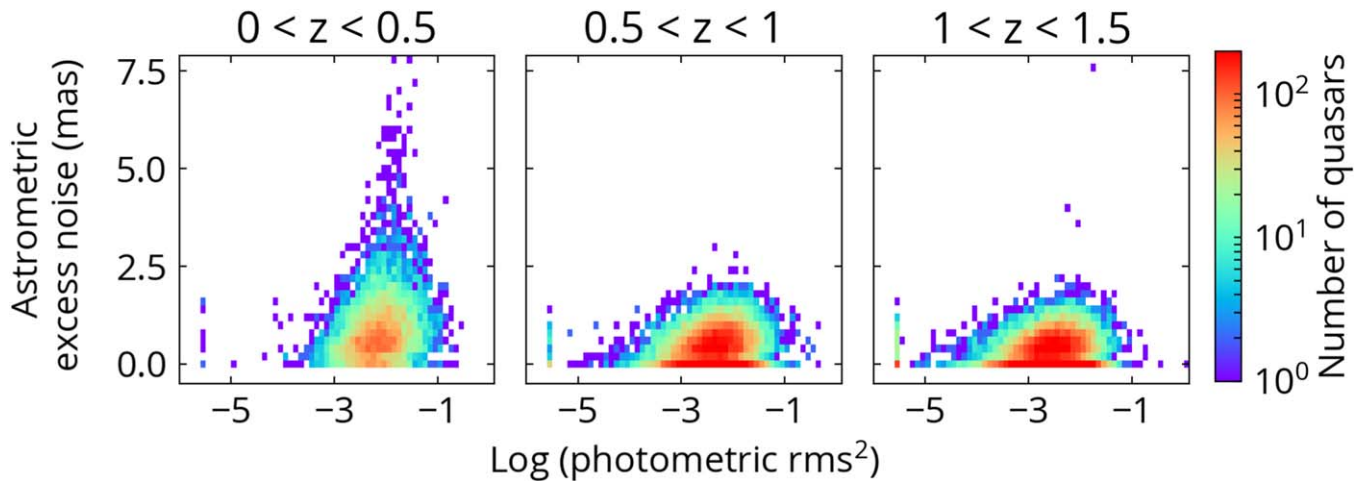
Figure 9. *Gaia* `astrometric_excess_noise` vs. photometric variability for spectroscopic SDSS quasars in three redshift ranges. There is a tail extending to high `astrometric_excess_noise` in the sample of $z < 0.5$. The tail is caused by extended host galaxies at lower redshifts and is not seen at higher redshifts. Quasars with high `astrometric_excess_noise` at redshifts >0.5 may be the subkiloparsec dual/lensed AGN candidates. The mild correlation between astrometric excess noise and variability is likely due to covariance in the measurements, e.g., both rms values are measured from fluxes in the same bandpass and measuring window. The locus of the distribution suggests that there is a floor level of ∼1 mas for the reliability of `astrometric_excess_noise`.

4.3. Varstrometry for Quasars

Figure 9 shows the distribution of SDSS quasars in the `astrometric_excess_noise` versus fractional photometric variability plane, for three redshift ranges. Here we only consider quasars that have a single *Gaia* matched source within $3''$, are brighter than 19.5 mag in *G* band, and have `visibility_periods_used` $\geqslant 9$ so that *Gaia* DR2 has sufficient number of observations for photometric and astrometric rms measurements. These additional cuts result in ∼86,000 SDSS quasars out of the parent ∼350,000 sample with *Gaia* matches. For sources where the variability is insignificant compared to the instrumental correction (i.e., $f_{G,\mathrm{raw}} \leqslant f_{G,\mathrm{inst}}$), we place them in the leftmost column of the plots. For the $z < 0.5$ sample, there is a long tail at $\log(f_G^2) \sim -2$ extending to high `astrometric_excess_noise`. The samples at $0.5 < z < 1$ and $1 < z < 1.5$ have very similar distributions in Figure 9, and neither of them displays a tail toward high astrometric noise seen in the $z < 0.5$ sample. This tail of high `astrometric_excess_noise` has values similar to those seen in the inactive galaxy sample (Section 3.2 and Figure 5), and thus it is mostly due to the extended structure (still treated as a single source in *Gaia* DR2) of the host galaxies that becomes more prominent at low redshifts. This effect of host galaxies seems insignificant for bright ($G < 19.5$ mag) quasars at $z > 0.5$. This trend is expected because (1) SDSS probes more luminous quasars at higher redshifts that dominate the total flux, (2) the angular sizes of the host galaxies are smaller at higher redshifts, and (3) host galaxies are very faint in the rest-frame UV at high redshifts and contribute much less to the total flux measured by *Gaia* than at lower redshifts.

Figure 9 also reveals a mild correlation between the photometric rms and `astrometric_excess_noise`, which we believe is due to the covariance in the astrometric and photometric rms estimates from the same data. For example, any residual host galaxy systematics resulting from window sizes and scanning directions of *Gaia* measurements increase both the photometric rms and astrometric rms estimates. The locus of the distribution in Figure 9 therefore

roughly defines a "floor" value of reliable `astrometric_excess_noise` around ∼1 mas for quasars, below which we do not consider the intrinsic astrometric rms estimate reliable.

Among ∼37,000 quasars with redshifts of 0.5–1.5, 6% have `astrometric_excess_noise` > 1 mas, and they tend to have photometric variability at the ∼10% level. This `astrometric_excess_noise` is difficult to explain with host galaxies in this redshift range. These quasars may be the subkiloparsec dual/off-nucleus AGNs and lensed AGNs that we are interested in. Confirming (i.e., resolving) them at <100 mas imaging resolution may be challenging. But at the very least, these astrometric rms estimates place stringent limits on the off-nucleus distance of these small-scale pairs (e.g., Shen et al. 2019).

We inspect the optical spectra and images of quasars at redshifts > 0.5 with `astrometric_excess_noise` > 2.5 mas. In the redshift range $0.5 < z < 1$, two sources, SDSS J123913.86+281434.1 and SDSS J112101.30+080926.3, have astrometric excess noise of 3.1 and 2.9 mas, respectively. Both of them show arguably double-peaked [O III] $\lambda5007$, and SDSS J112101.30+080926.3 clearly has an asymmetric broad [O III] $\lambda5007$ emission (Figure 10). The asymmetric broad [O III] profile could be due to a galactic wind (e.g., Zakamska & Greene 2014) or a double-peaked [O III] from a dual AGN (e.g., Liu et al. 2018). Their optical images in Pan-STARRS show that both of them have red faint sources within ∼3″ that are not detected by *Gaia*. These red sources may be foreground stars, merger companions of the quasar, or tidal streams. Even though these close red sources are undetected in *Gaia*, we are unable to rule out the possibility that the `astrometric_excess_noise` may be caused by these faint sources. Also, these two quasars happen to have redshifts of 0.52 and 0.51, and it is possible that their host galaxies may contribute to some uncertainties in the astrometric rms.

There are three quasars with astrometric excess noise >2.5 mas at redshift $1 < z < 1.5$. Their SDSS spectra clearly show quasar broad-line features, with no trace of stellar spectra from chance superposition with a foreground star. Figure 11 presents one example, SDSS J000252.60–034345.1, that has an `astrometric_excess_noise` of 3.7 mas at $z = 1.39$. In
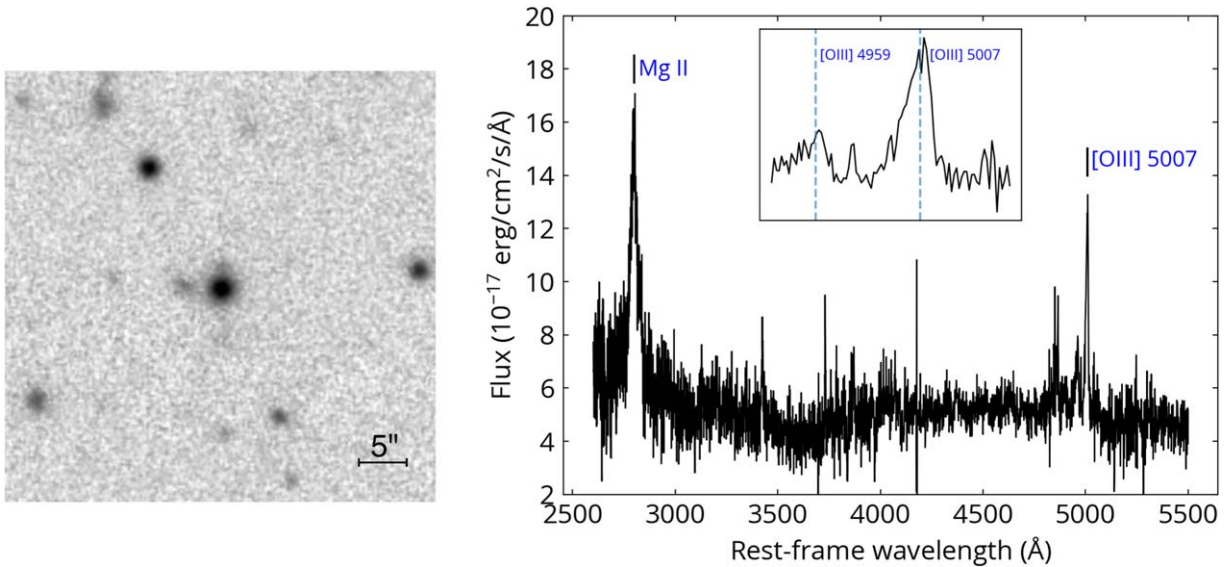
Figure 10. Pan-STARRS *i*-band optical image (north/east is up/left) and SDSS spectrum of SDSS J112101.30+080926.3, a quasar (centered in the image) that has an astrometric excess noise of 2.9 mas at $z = 0.51$. The *i*-band image shows some faint companions around the quasar, one to the north and one to the east. Its [O III] λ5007 narrow emission line shows an asymmetric profile (when zoomed in) that may be caused by multiple kinematic components associated with a dual AGN.
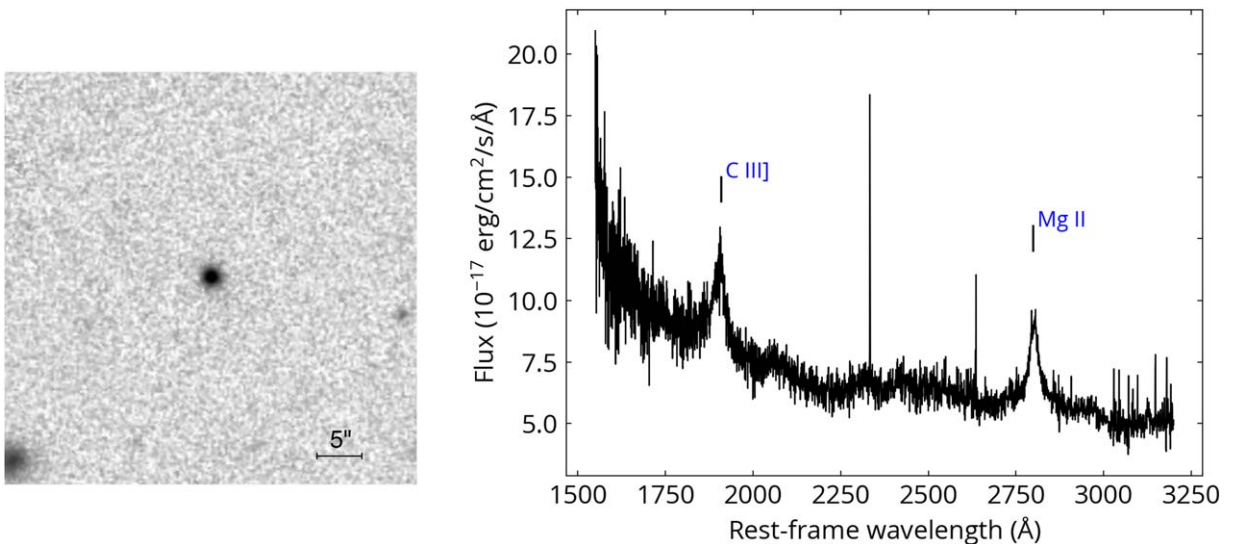

Figure 11. Pan-STARRS *i*-band optical image (north/east is up/left) and SDSS spectrum (right panel) of SDSS J000252.60−034345.1, a quasar (centered in the image) that has an `astrometric_excess_noise` of 3.7 mas at $z = 1.39$. No source is strongly detected within 20″ around the quasar down to Pan-STARRS limiting magnitude of 23.1.

its *i*-band image from Pan-STARRS 1 (left panel), there is no detected extended host or companion within 15″ that can affect the astrometric measurements. If its `astrometric_excess_noise` is from an unresolved equal-flux dual AGN, Equation (2) implies a projected separation of 81 mas, or 700 pc at its redshift.

4.4. Extension to the WISE Quasar Sample

So far, we have used the spectroscopic quasar sample from SDSS to reduce source contamination. To increase the sky overlap with *Gaia*, we use an all-sky quasar sample selected using *WISE* data and presented in Mateos et al. (2012) and Secrest et al. (2015). These *WISE*-selected photometric quasars are used by *Gaia* to define the celestial frame (Gaia Collaboration et al. 2018b; Lindegren et al. 2018). While most

of them should be genuine quasars, not all of them are spectroscopically confirmed and have known redshifts. Similar to the SDSS quasar sample, here we only consider *WISE*-selected quasars that are brighter than 19.5 mag in *G* band and have `visibility_periods_used > 8`.

Here we use a subset of these *WISE* quasars to demonstrate the varstrometry selection of candidate subkiloparsec dual/off-nucleus AGNs and the utility of *Gaia* to select blazars. We first limit the *WISE* quasar sample to those that Pan-STARRS 1 flags as point sources in all filters to reduce the systematics caused by extended host galaxies. To include radio information, we cross-match the sample with the catalog of Faint Images of the Radio Sky at Twenty cm (FIRST; Becker et al. 1995; White et al. 1997) with a matching radius of 3″. In this cross-match procedure, sources with strong radio lobes but weak compact cores may be missed. Because sources with
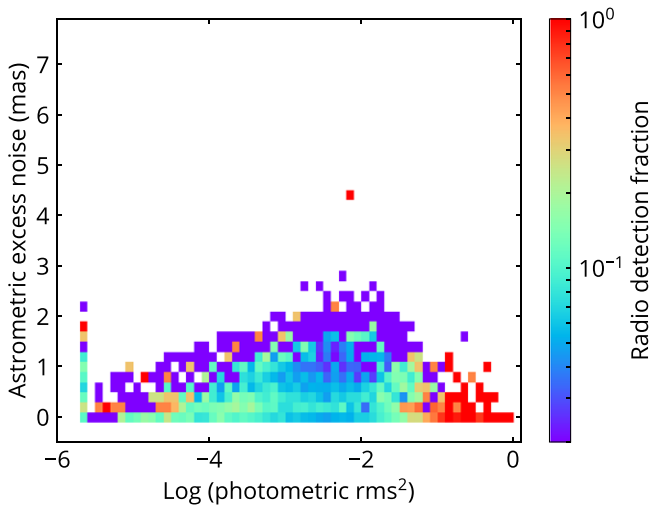
Figure 12. Radio detection fraction for *WISE*-selected quasars that are classified as point source in Pan-STARRS and are within the FIRST footprint. Compared to Figure 9, one significant difference is that the *WISE*-selected sample has more highly variable (fractional photometric rms >30%) blazars with a high radio detection fraction but low `astrometric_excess_noise`.

radio lobes only compose ≲10% of all radio sources in FIRST (e.g., van Velzen et al. 2015), this does not affect our main conclusion.

In Figure 12, we present the radio detection fraction in FIRST for the *WISE*-selected quasar sample. One significant difference between the spectroscopic SDSS quasars in Figure 9 and *WISE*-selected quasars in Figure 12 is that *WISE*-selected quasars retain a larger number of strongly variable sources $(\log(f_G^2) > -1)$. Figure 12 shows that these strongly variable sources have very high radio detection fractions but low `astrometric_excess_noise`. These strongly variable sources may be blazars or flat-spectrum radio quasars, and the properties of variability-selected extragalactic sources in *Gaia* are currently being investigated (J. C. Isler et al. 2019, in preparation).

A few strongly variable sources $(\log(f_G^2) > -1)$ still have `astrometric_excess_noise` > 1 mas. If the astrometric jitter is caused by the superluminal motion of the jet, it requires a minimal Lorentz factor of 50 to explain a jitter of ∼1 mas, and the jet has to be propagating within an angle of 0.02 rad to the line of sight. In addition to that, the jet has to be extended and optically bright enough to induce significant astrometric jitter, which is difficult. Alternatively, the astrometric rms can be due to variable subkiloparsec jets and knots in the optical, or genuine dual/off-nucleus AGNs. We plan to investigate these systems in a follow-up study.

5. Discussion

5.1. Merits and Limitations of `Varstrometry`

We have laid out the working principles of `varstrometry` in the context of finding stationary (position-wise), unresolved offset or dual AGN systems where the photocenter varies along with photometric variations. The expected astrometric signal at fixed pair separation is strongest when the members of the unresolved source are highly variable and have comparable fluxes. The most significant advantage of this technique is its ability to explore AGN separations below ∼1 kpc, utilizing the superb astrometric precision from

astrometry missions like *Gaia*. The technique may also have a broader application in general, e.g., to probe Galactic stellar binary systems (e.g., Makarov & Goldin 2016).

Using `varstrometry` and the all-sky *Gaia* data, we can perform systematic searches of subkiloparsec off-nucleus and dual AGNs and compare with predictions from simulations. For example, some galaxy formation simulations predict a large number of wandering active SMBHs in the host galaxy during the inspiraling phase (e.g., Tremmel et al. 2018), and this population of off-nucleus AGNs can be best constrained by this `varstrometry` technique and *Gaia* data. In a similar spirit we can also confront the observational constraints using this technique with the predicted population of recoiling SMBHs in simulations (e.g., Blecha et al. 2016) to test the kick velocity distribution, correlations with galactic potential, and accretion recipes in these simulations. Another application is strong gravitationally lensed quasars with closely separated multiple images below ∼0.″2 *Gaia* resolution: because of the time delays in the intrinsic quasar variability between these gravitationally lensed images (Blandford & Narayan 1992), we will observe similar astrometric jitter in the source photocenter. In the future with much higher astrometric precisions (e.g., μas; Vallenari 2018), it may even be possible to apply `varstrometry` to the variable broad-line region of quasars (e.g., Shen 2012) to independently constrain the broad-line region size.

The major limitation of this technique is that it only applies to systems where at least one offset member is an optically unobscured AGN to ensure photometric variability of the system. Especially, an enhanced level of AGN obscuration in late-stage mergers has been reported in literature (Satyapal et al. 2014; Ricci et al. 2017). In addition, for the induced astrometric signature to be detectable given the astrometric precision, it requires a suitable combination of pair separation (or off-nucleus distance), flux ratio, and photometric variability amplitude (Equations (3)–(5)).

There are also technical limitations of the application of `varstrometry` that are specific to *Gaia*. We have shown that extended hosts (albeit still treated as point source in *Gaia* DR2) may impact the quality of *Gaia* astrometry and the interpretation of the reported `astrometric_excess_noise`. Thus, follow-up observations, with sufficient spatial resolution to resolve the tentative subkiloparsec pair, are required to confirm *Gaia*-selected candidates. *Gaia* DR2 does not release time series of photocenter measurements and light curves; hence, we can only use proxies in the *Gaia* DR2 catalog to approximate the (intrinsic) photometric and astrometric rms. Ideally we require a full understanding and characterization of the systematics in the measured astrometric rms, at a level that will make the `varstrometry` technique competitive. For example, if we can control the total systematic astrometric rms to less than a few mas, we can confidently attribute a large measured astrometric rms to the `varstrometric` signal.

Another case where we can confidently confirm an off-nucleus AGN+galaxy system with `varstrometry` alone is where the photocenter variations are aperiodic, bound, and linear and correlate with the photometric light curve (Section 2.2). Time series from *Gaia* are required for such analyses.

5.2. Follow-up Strategy

To further explore systematics in *Gaia* astrometry, and to confirm candidate subkiloparsec dual or off-nucleus AGNs selected from *Gaia* DR2, we require high-resolution imaging

follow-up observations. Additional observations, such as spatially resolved spectroscopy, are also important to reduce ambiguities. Below we discuss our follow-up strategy.

Gaia provides many resolved pairs at $\gtrsim 0\rlap{.}''3$ scales; most of them are foreground stars, but some of them may be off-nucleus or dual AGNs on ~ 1–10 kpc scales. For AGNs with multiple *Gaia* detections within $3''$ ($D \sim 0\rlap{.}''3$–$3''$), the following candidates are of high priority:

1. targets with resolved *Gaia* sources that are consistent with AGNs in terms of color, variability, and parallax (proper motion) measurements—to remove most contaminants from foreground stars;
2. targets with radio detection—to facilitate high-resolution imaging with radio interferometry.

For <1 kpc candidates selected with `varstrometry` from unresolved *Gaia* sources ($D \lesssim 0\rlap{.}''3$), the following candidates are of high priority:

1. targets with less extended morphology from ground-based seeing-limited imaging—to mitigate *Gaia* DR2 systematics on extended sources;
2. targets whose expected separation is resolvable, i.e., those with large photometric and astrometric rms, or significant parallax and/or proper-motion detections;
3. targets with significant color variability—to increase the probability of dual/off-nucleus AGNs;
4. targets with radio detection because dual/off-nucleus radio-loud AGNs are suitable targets for VLBI imaging.

In addition, for those with spatially integrated fiber spectroscopy from SDSS (within $3''$ or $2''$ fiber diameter), candidates with obvious AGN–star superposition are not considered. These follow-up strategies are designed to improve the overall success rate of confirmation and also to explore additional systematics from *Gaia* DR2.

6. Summary and Conclusions

In this paper, we have introduced a new technique, `varstrometry`, based on the ideas proposed in Shen (2012) and Liu (2015), where astrometric jitter induced by intrinsic photometric variability in unresolved off-center sources can be used to constrain the pair separation. A particular application of this technique is to identify sub-kiloparsec dual and off-nucleus AGNs with milliarcsecond-precision astrometry. We present the basic principles of this technique and explore its feasibility and potential systematics using *Gaia* DR2. Our main results are as follows:

1. Candidate subkiloparsec dual or off-nucleus AGNs can be identified based on *Gaia*-detected photocenter variations that are bound, linear, and aperiodic. If there is further a strong correlation between the photocenter shift and the total flux variability, it will signal a single off-nucleus AGN that dominates the variable light. If the host light can be further derived from spectral or imaging decomposition in any epoch, the time series of the photocenter and flux measurements can be used to fit for the pair separation via Equation (4).
2. If only rms measurements of the photocenter and fluxes are available, one can still derive an estimate of the pair separation or off-nucleus distance via Equations (3) and

(5) for the dual AGN case and the off-nucleus single AGN case, respectively.

3. We use pre-main-sequence stars that have *Gaia*-unresolved companions to test the feasibility of `varstrometry` in *Gaia* DR2. In general, the observed astrometric rms is consistent with the expectation from `varstrometry` (Figure 6), supporting that we are indeed seeing the variability-induced astrometric rms that can be constrained by *Gaia*.
4. We show that extended host galaxies (albeit still treated as point sources in *Gaia* DR2) with $R_{50} > 1''$ have extra systematic photometric rms of $\sim 15\%$ and astrometric rms of ~ 10 mas in *Gaia* DR2 (Figure 5). This may be improved for future *Gaia* data releases with better treatments for extended sources. In *Gaia* DR2, the effect of extended host galaxies is important for quasars at $z \lesssim 0.5$.
5. We investigate the astrometric and photometric rms properties of spectroscopically confirmed quasars from SDSS and present several example candidates that are potentially genuine subkiloparsec dual or off-nucleus AGNs. There are at least hundreds of good subkiloparsec dual/off-nucleus AGN candidates with `astrometric_excess_noise` $\gtrsim 2$ mas where the follow-up efforts should be centered. We also explore the properties of *WISE*-selected photometric quasars and identify a large number of blazar candidates based on *Gaia* photometric variability (Figure 12).
6. We discuss the merits and main limitations of this technique, as well as our follow-up strategies for promising candidates (Section 5).

In future work, we will further explore the utility of the combination of `varstrometry` and *Gaia* data. For example, we have applied this technique to statistically constrain the subkiloparsec off-nucleus AGN population at low redshift (Shen et al. 2019). We are planning follow-up observations to observe our most promising candidates selected from *Gaia* that are potentially genuine subkiloparsec dual AGNs, off-nucleus AGNs, or gravitational lenses.

With future *Gaia* releases that provide time series of photocenter and light curves, we will be able to refine the selection by computing rms directly from time series and by cross-correlating photocenter and flux variability. Extended time baselines from *Gaia* will also improve the detection of photocenter variations (e.g., more frequent large-amplitude AGN variations on longer timescales) and facilitate the cross-correlation analysis between photocenter positions and light curves. Refined treatments for extended sources will also help mitigate the systematics on *Gaia* astrometric rms estimation. In the meantime, our follow-up observations will help provide a better understanding of *Gaia* systematics and thus facilitate the application of `varstrometry`.

Appendix

Here we provide summary tables, optical images from Pan-STARRS, and SDSS spectra for genuine quasars that have significant nonzero parallaxes or proper motions from *Gaia* DR2. We summarize quasars with significant parallax detections in Table 2 and those with significant proper-motion detections in Table 3. The *Gaia* coordinates in these tables have a precision of ∼0.04 mas. Figures 13–16 are the Pan-STARRS optical images and the SDSS spectra for sources in Tables 2 and 3. The red circles in the Pan-STARRS images are all *Gaia* DR2 detections at the J2015.5 epoch. Images have 10″ on each side.
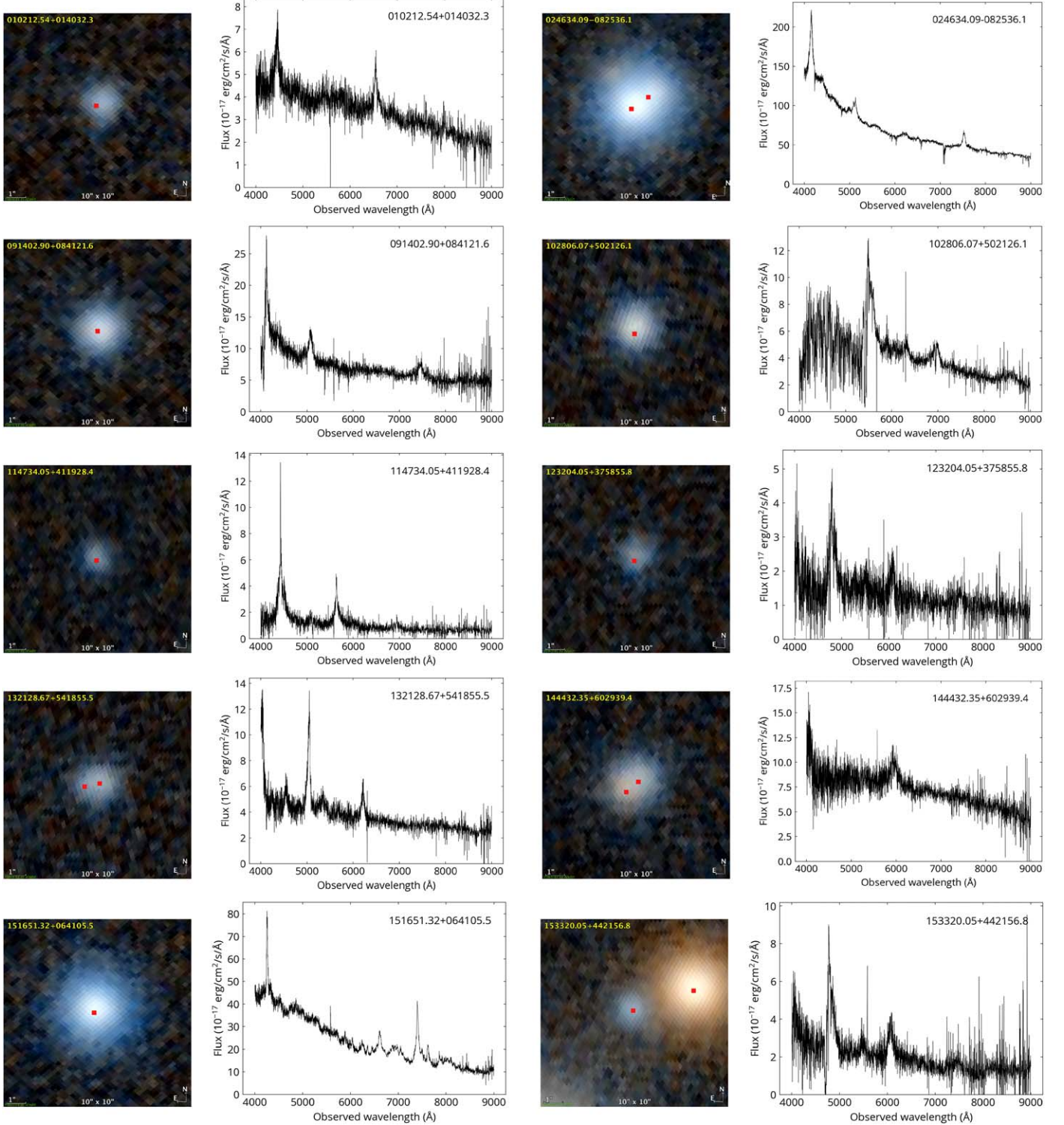

Figure 13. Pan-STARRS 1 color-composite images (left) and SDSS spectra (right) for genuine quasars with nonzero parallaxes from *Gaia* DR2. The red circles in the Pan-STARRS images are the *Gaia* detections at the J2015.5 epoch. Images have 10″ on each side, and north (east) is up (left).
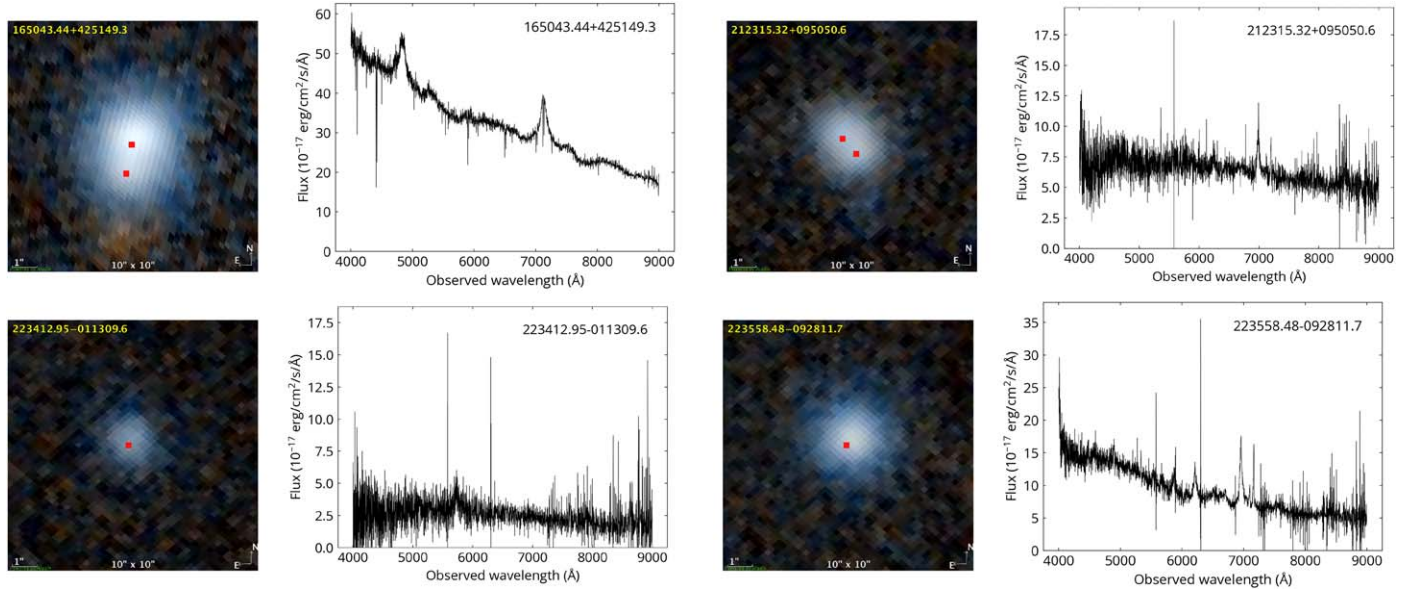
Figure 14. Same as Figure 13, but for a different set of objects.

Table 2
List of Genuine Quasars That Have Significant Nonzero Parallaxes from *Gaia* DR2

SDSS Name	R.A. (deg)	Decl. (deg)	Parallax (mas)	parallax_over_error
010212.54+014032.3	15.55226876	1.67566157	3.49	5.96
024634.09−082536.1	41.64186178	−8.42654860	nan	nan
	41.64211573	−8.42672206	1.63	6.80
091402.90+084121.6	138.51208139	8.68936409	1.61	5.05
102806.07+502126.1	157.02533446	50.35723731	2.53	7.07
114734.05+411928.4	176.89189707	41.32453769	7.18	5.59
123204.05+375855.8	188.01691412	37.98213972	8.15	5.06
132128.67+541855.5	200.36940864	54.31544109	4.92	6.44
	200.36978657	54.31539680	nan	nan
144432.35+602939.4	221.13473179	60.49432884	7.35	7.59
	221.13508711	60.49417643	0.92	0.80
151651.32+064105.5	229.21388692	6.68486792	6.25	6.15
153320.05+442156.8	233.33356955	44.36581427	3.98	6.01
165043.44+425149.3	252.68110564	42.86339288	0.43	0.86
	252.68102328	42.86371533	0.91	5.40
212315.32+095050.6	320.81378486	9.84730542	nan	nan
	320.81394408	9.84747621	5.29	5.30
223412.95−011309.6	338.55400872	−1.21933023	13.96	9.20
223558.48−092811.7	338.99368620	−9.46991281	4.09	5.82

Note. Positions are also from *Gaia* DR2 and have precisions of ∼0.04 mas. Some SDSS quasars have two *Gaia* matches within 1″.

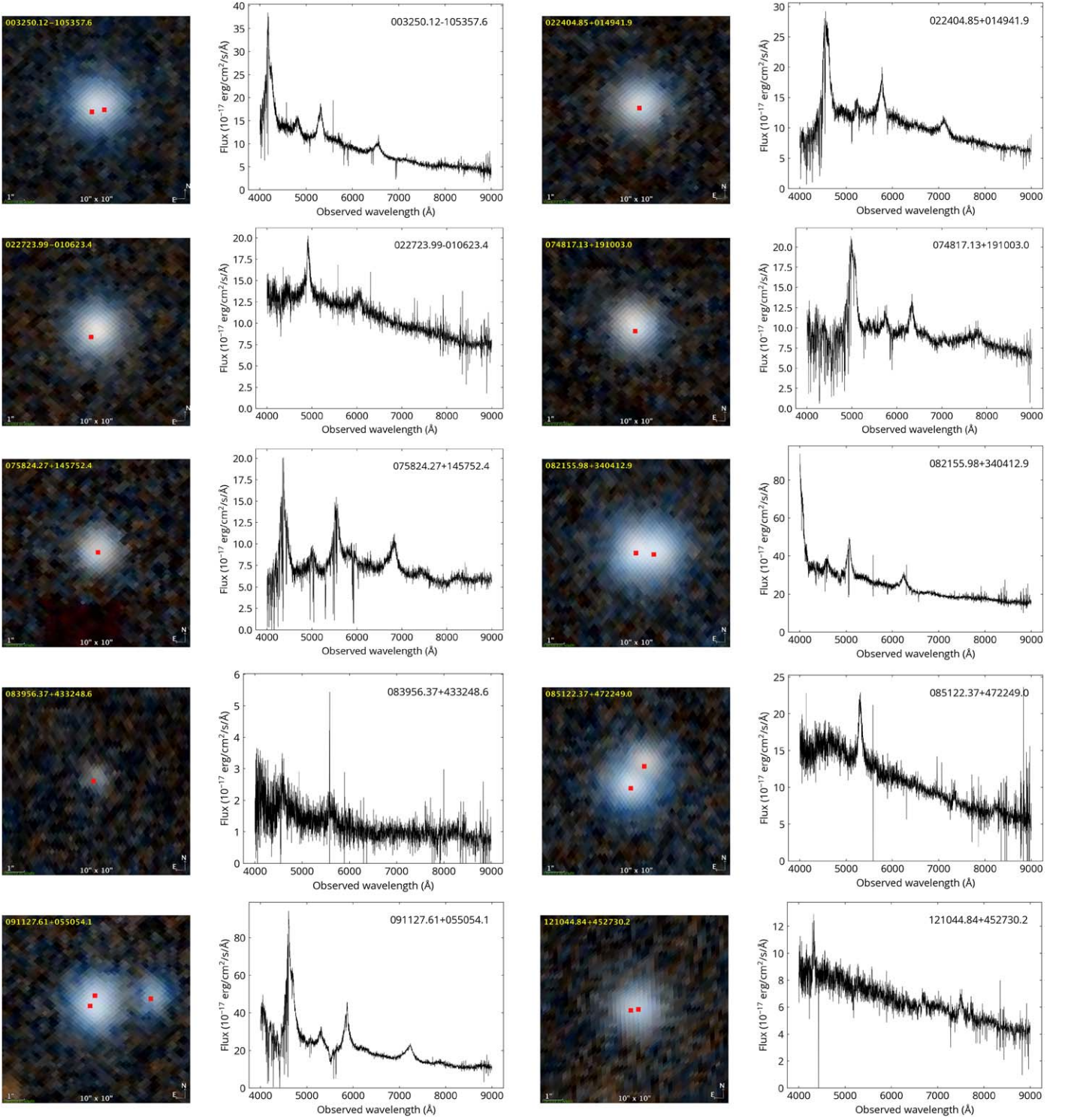(This table is available in its entirety in machine-readable form.)

Figure 15. Pan-STARRS 1 color-composite images (left) and SDSS spectra (right) for genuine quasars with nonzero proper motions from *Gaia* DR2. The red circles in the Pan-STARRS images are the *Gaia* detections at the J2015.5 epoch. Images have 10″ on each side, and north (east) is up (left).
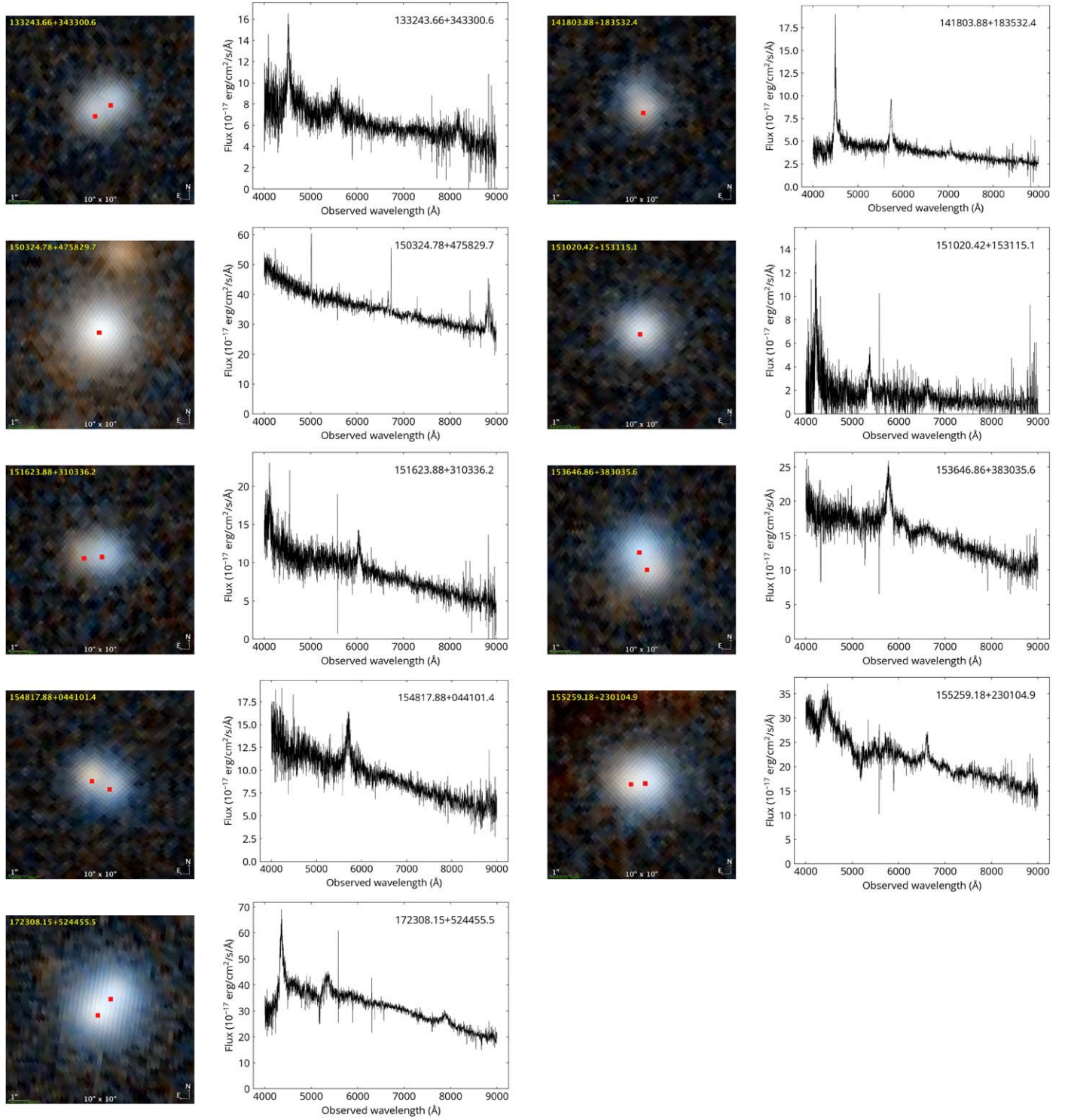
Figure 16. Same as Figure 15, but for a different set of objects.

Table 3
List of Genuine Quasars That Have Significant Nonzero Proper Motions from *Gaia* DR2

SDSS Name	R.A. (deg)	Decl. (deg)	Total Proper Motion mas yr^{-1}	pm_over_error
003250.12−105357.6	8.20890136	−10.89935725	22.44	14.00
	8.20871290	−10.89932825	…	
022404.85+014941.9	36.02016279	1.82833372	7.51	10.55
022723.99−010623.4	36.85003493	−1.10656877	30.30	27.79
074817.13+191003.0	117.07139158	19.16751662	11.92	16.53
075824.27+145752.4	119.60109938	14.96456712	12.55	11.92
082155.98+340412.9	125.48325872	34.07025103	3.55	5.42
	125.48293423	34.07023015	7.97	22.73
083956.37+433248.6	129.98492865	43.54683719	43.52	13.65
085122.37+472249.0	132.84303687	47.38050201	9.24	13.68
	132.84332839	47.38017838	0.20	0.67
091127.61+055054.1	137.86506252	5.84856614	…	
	137.86513579	5.84840999	10.39	10.82
121044.84+452730.2	182.68691512	45.45837117	11.43	13.16
	182.68675057	45.45839074	…	
133243.66+343300.6	203.18173257	34.55023612	0.32	0.52
	203.18200803	34.55007318	22.71	28.02
141803.88+183532.4	214.51614365	18.59229451	13.47	16.04
150324.78+475829.7	225.85327225	47.97495113	3.05	14.40
151020.42+153115.1	227.58511015	15.52087067	8.48	20.85
151623.88+310336.2	229.09947298	31.06009574	0.61	1.51
	229.09978114	31.06007692	33.90	19.52
153646.86+383035.6	234.19514960	38.50974338	9.03	18.29
	234.19529623	38.50999595	7.75	7.58
154817.88+044101.4	237.07436189	4.68365592	…	
	237.07462435	4.68377879	18.97	18.62
155259.18+230104.9	238.24675652	23.01803655	7.51	20.85
	238.24653013	23.01804974	1.03	1.95
172308.15+524455.5	260.78401847	52.74866790	9.66	47.75
	260.78370514	52.74890673	0.14	0.49

Note. Positions are also from *Gaia* DR2 and have precisions of ∼0.04 mas. Some SDSS quasars have two *Gaia* matches within 1″.

(This table is available in its entirety in machine-readable form.)

ORCID iDs

Hsiang-Chih Hwang ⓘ https://orcid.org/0000-0003-4250-4437
Yue Shen ⓘ https://orcid.org/0000-0003-1659-7035
Nadia Zakamska ⓘ https://orcid.org/0000-0001-6100-6869
Xin Liu ⓘ https://orcid.org/0000-0003-0049-5210

References

Aihara, H., AlSayyad, Y., Ando, M., et al. 2019, PASJ, in press
Arenou, F., Luri, X., Babusiaux, C., et al. 2018, A&A, 616, A17
Bailey, J. 1998, MNRAS, 301, 161
Baker, J. G., Centrella, J., Choi, D.-I., et al. 2006, ApJL, 653, L93
Baldwin, J. A., Phillips, M. M., & Terlevich, R. 1981, PASP, 93, 5
Bansal, K., Taylor, G. B., Peck, A. B., Zavala, R. T., & Romani, R. W. 2017, ApJ, 843, 14
Barrows, R. S., Comerford, J. M., Greene, J. E., & Pooley, D. 2017, ApJ, 838, 129
Barth, A. J., Bentz, M. C., Greene, J. E., & Ho, L. C. 2008, ApJL, 683, L119
Barth, A. J., & Stern, D. 2018, ApJ, 859, 10
Becker, R. H., White, R. L., & Helfand, D. J. 1995, ApJ, 450, 559
Begelman, M. C., Blandford, R. D., & Rees, M. J. 1980, Natur, 287, 307
Belokurov, V., Erkal, D., Deason, A. J., et al. 2017, MNRAS, 466, 4711
Belokurov, V. A., & Evans, N. W. 2002, MNRAS, 331, 649
Blaes, O., Lee, M. H., & Socrates, A. 2002, ApJ, 578, 775
Blandford, R. D., & Narayan, R. 1992, ARA&A, 30, 311
Blecha, L., Sijacki, D., Kelley, L. Z., et al. 2016, MNRAS, 456, 961
Bogdanović, T. 2015, ASSP, 40, 103
Bogdanović, T., Reynolds, C. S., & Miller, M. C. 2007, ApJL, 661, L147
Britzen, S., Fendt, C., Witzel, G., et al. 2018, MNRAS, 478, 3199
Burke-Spolaor, S. 2011, MNRAS, 410, 2113
Centrella, J., Baker, J. G., Kelly, B. J., & van Meter, J. R. 2010, RvMP, 82, 3069
Chambers, K. C., Magnier, E. A., Metcalfe, N., et al. 2016, arXiv:1612.05560
Charisi, M., Bartos, I., Haiman, Z., et al. 2016, MNRAS, 463, 2145
Civano, F., Elvis, M., Lanzuisi, G., et al. 2010, ApJ, 717, 209
Civano, F., Elvis, M., Lanzuisi, G., et al. 2012, ApJ, 752, 49
Collinge, M. J., Strauss, M. A., Hall, P. B., et al. 2005, AJ, 129, 2542
Colpi, M., & Dotti, M. 2011, ASL, 4, 181
Comerford, J. M., & Greene, J. E. 2014, ApJ, 789, 112
Comerford, J. M., Pooley, D., Barrows, R. S., et al. 2015, ApJ, 806, 219
Diehl, H. T., Neilsen, E., Gruendl, R., et al. 2016, Proc. SPIE, 9910, 99101D
D'Orazio, D. J., Haiman, Z., & Schiminovich, D. 2015, Natur, 525, 351
Dosopoulou, F., & Antonini, F. 2017, ApJ, 840, 31
Dotti, M., Sesana, A., & Decarli, R. 2012, AdAst, 2012, 940568
Ducourant, C., Wertz, O., Krone-Martins, A., et al. 2018, A&A, 618, 56
Eracleous, M., Boroson, T. A., Halpern, J. P., & Liu, J. 2012, ApJS, 201, 23
Eracleous, M., & Halpern, J. P. 1994, ApJS, 90, 1
Evans, D. W., Riello, M., De Angeli, F., et al. 2018, A&A, 616, A4
Event Horizon Telescope Collaboration, Akiyama, K., Alberdi, A., et al. 2019, ApJL, 875, L2
Fu, H., Myers, A. D., Djorgovski, S. G., et al. 2015a, ApJ, 799, 72
Fu, H., Wrobel, J. M., Myers, A. D., Djorgovski, S. G., & Yan, L. 2015b, ApJL, 815, L6
Fu, H., Yan, L., Myers, A. D., et al. 2012, ApJ, 745, 67
Gaia Collaboration, Brown, A. G. A., Vallenari, A., et al. 2018a, A&A, 616, A1
Gaia Collaboration, Mignard, F., Klioner, S. A., et al. 2018b, A&A, 616, A14
Gaia Collaboration, Prusti, T., & de Bruijne, J. H. J. 2016, A&A, 595, 1
Gaskell, C. M. 1983, LIACo, 24, 473
Ghez, A. M., Neugebauer, G., & Matthews, K. 1993, AJ, 106, 2005

Ghez, A. M., White, R. J., & Simon, M. 1997, ApJ, 490, 353
Gould, A., & Rix, H.-W. 2000, ApJL, 532, L29
Goulding, A. D., Pardo, K., Greene, J. E., et al. 2019, ApJL, 879, L21
Graham, M. J., Djorgovski, S. G., Stern, D., et al. 2015a, MNRAS, 453, 1562
Graham, M. J., Djorgovski, S. G., Stern, D., et al. 2015b, Natur, 518, 74
Gravity Collaboration, Sturm, E., Dexter, J., et al. 2018, Natur, 563, 657
Guo, H., Liu, X., Shen, Y., et al. 2019, MNRAS, 482, 3288
Haehnelt, M. G. 1994, MNRAS, 269, 199
Hu, W., Barkana, R., & Gruzinov, A. 2000, PhRvL, 85, 1158
Hughes, S. A. 2009, ARA&A, 47, 107
Hui, L., Ostriker, J. P., Tremaine, S., & Witten, E. 2017, PhRvD, 95, 043541
Hwang, H.-C., & Zakamska, N. 2019, arXiv:1909.06375
Jaffe, A. H., & Backer, D. C. 2003, ApJ, 583, 616
Kauffmann, G., Heckman, T. M., Tremonti, C., et al. 2003, MNRAS, 346, 1055
Kelley, L. Z., Blecha, L., & Hernquist, L. 2017, MNRAS, 464, 3131
Kelly, B. C. 2007, ApJ, 665, 1489
Kewley, L. J., Dopita, M. A., Sutherland, R. S., Heisler, C. A., & Trevena, J. 2001, ApJ, 556, 121
Khan, F. M., Holley-Bockelmann, K., Berczik, P., & Just, A. 2013, ApJ, 773, 100
Kharb, P., Lal, D. V., & Merritt, D. 2017, NatAs, 1, 727
Kohler, R., & Leinert, C. 1998, A&A, 331, 977
Komossa, S., Burwitz, V., Hasinger, G., et al. 2003, ApJL, 582, L15
Kristian, J., Groth, E. J., Shaya, E. J., et al. 1993, AJ, 106, 1330
Laury-Micoulaut, C. A. 1976, A&A, 51, 343
Leinert, C., Zinnecker, H., Weitzel, N., et al. 1993, A&A, 278, 129
Lemon, C. A., Auger, M. W., McMahon, R. G., & Koposov, S. E. 2017, MNRAS, 472, 5023
Li, Y.-R., Wang, J.-M., Ho, L. C., et al. 2016, ApJ, 822, 4
Lindegren, L. 1978, in IAU Colloq. 48, Modern Astrometry, ed. F. V. Prochazka & R. H. Tucker (Vienna: Vienna Univ. Observatory), 197
Lindegren, L., Hernández, J., Bombrun, A., et al. 2018, A&A, 616, A2
Lindegren, L., Lammers, U., Hobbs, D., et al. 2012, A&A, 538, A78
Liu, T., Gezari, S., Ayers, M., et al. 2019, ApJ, 884, 36
Liu, X., Greene, J. E., Shen, Y., & Strauss, M. A. 2010, ApJL, 715, L30
Liu, X., Guo, H., Shen, Y., Greene, J. E., & Strauss, M. A. 2018, ApJ, 862, 29
Liu, X., Shen, Y., Bian, F., Loeb, A., & Tremaine, S. 2014, ApJ, 789, 140
Liu, Y. 2015, A&A, 580, A133
Liu, Y. 2016, A&A, 592, L4
MacLeod, C. L., Ivezić, Ž., Sesar, B., et al. 2012, ApJ, 753, 106
Magain, P., Surdej, J., Swings, J. P., Borgeest, U., & Kayser, R. 1988, Natur, 334, 325
Makarov, V. V., & Goldin, A. 2016, ApJS, 224, 19
Mateos, S., Alonso-Herrero, A., Carrera, F. J., et al. 2012, MNRAS, 426, 3271

Merritt, D. 2013, Dynamics and Evolution of Galactic Nuclei (Princeton, NJ: Princeton Univ. Press)
Milosavljević, M., & Merritt, D. 2001, ApJ, 563, 34
Müller-Sánchez, F., Comerford, J., Stern, D., & Harrison, F. A. 2016, ApJ, 830, 50
Nguyen, D. C., Brandeker, A., van Kerkwijk, M. H., & Jayawardhana, R. 2012, ApJ, 745, 119
Pâris, I., Petitjean, P., Aubourg, É., et al. 2018, A&A, 613, A51
Ricci, C., Bauer, F. E., Treister, E., et al. 2017, MNRAS, 468, 1273
Rodriguez, C., Taylor, G. B., Zavala, R. T., et al. 2006, ApJ, 646, 49
Satyapal, S., Ellison, S. L., McAlpine, W., et al. 2014, MNRAS, 441, 1297
Secrest, N. J., Dudik, R. P., Dorland, B. N., et al. 2015, ApJS, 221, 12
Sesar, B., Ivezić, Ž., Lupton, R. H., et al. 2007, AJ, 134, 2236
Shen, Y. 2012, ApJ, 757, 152
Shen, Y., Hwang, H.-C., Zakamska, N., & Liu, X. 2019, ApJL, 885, L4
Shen, Y., Liu, X., Greene, J. E., & Strauss, M. A. 2011a, ApJ, 735, 48
Shen, Y., Liu, X., Loeb, A., & Tremaine, S. 2013, ApJ, 775, 49
Shen, Y., & Loeb, A. 2010, ApJ, 725, 249
Shen, Y., Richards, G. T., Strauss, M. A., et al. 2011b, ApJS, 194, 45
Simon, M., Ghez, A. M., Leinert, C., et al. 1995, ApJ, 443, 625
Steinborn, L. K., Dolag, K., Comerford, J. M., et al. 2016, MNRAS, 458, 1013
Stern, J., Hennawi, J. F., & Pott, J.-U. 2015, ApJ, 804, 57
Strateva, I. V., Strauss, M. A., Hao, L., et al. 2003, AJ, 126, 1720
Thomas, D., Steele, O., Maraston, C., et al. 2013, MNRAS, 431, 1383
Tremmel, M., Governato, F., Volonteri, M., Quinn, T. R., & Pontzen, A. 2018, MNRAS, 475, 4967
Vallenari, A. 2018, FrASS, 5, 11
Valtonen, M. J. 2007, ApJ, 659, 1074
Vanden Berk, D. E., Wilhite, B. C., Kron, R. G., et al. 2004, ApJ, 601, 692
van Velzen, S., Falcke, H., & Körding, E. 2015, MNRAS, 446, 2985
Vaughan, S., Uttley, P., Markowitz, A. G., et al. 2016, MNRAS, 461, 3145
Volonteri, M., Bogdanović, T., Dotti, M., & Colpi, M. 2016, IAUFM, 29, 285
Volonteri, M., Haardt, F., & Madau, P. 2003, ApJ, 582, 559
Weymann, R. J., Latham, D., Angel, J. R. P., et al. 1980, Natur, 285, 641
White, R. L., Becker, R. H., Helfand, D. J., & Gregg, M. D. 1997, ApJ, 475, 479
Wielen, R. 1996, A&A, 314, 679
Wright, E. L., Eisenhardt, P. R. M., Mainzer, A. K., et al. 2010, AJ, 140, 1868
Young, P., Deverill, R. S., Gunn, J. E., Westphal, J. A., & Kristian, J. 1981, ApJ, 244, 723
Yu, Q. 2002, MNRAS, 331, 935
Yu, Q., Lu, Y., Mohayaee, R., & Colin, J. 2011, ApJ, 738, 92
Yuan, S., Strauss, M. A., & Zakamska, N. L. 2016, MNRAS, 462, 1603
Zakamska, N. L., & Greene, J. E. 2014, MNRAS, 442, 784
Zheng, Z.-Y., Butler, N. R., Shen, Y., et al. 2016, ApJ, 827, 56